

Forward doubly-virtual Compton scattering off the nucleon in chiral perturbation theory at NLO: the subtraction function and moments of unpolarized structure functions

Jose Manuel Alarcón

*Departamento de Física Teórica & IPARCOS,
Universidad Complutense de Madrid, 28040 Madrid, Spain*

Franziska Hagelstein

*Albert Einstein Center for Fundamental Physics,
Institute for Theoretical Physics, University of Bern,
Sidlerstrasse 5, CH-3012 Bern, Switzerland*

Vadim Lensky and Vladimir Pascalutsa

*Institut für Kernphysik & Cluster of Excellence PRISMA+,
Johannes Gutenberg-Universität Mainz, D-55128 Mainz, Germany*

(Dated: December 22, 2024)

Abstract

The forward doubly-virtual Compton scattering (VVCS) off the nucleon contains a wealth of information on nucleon structure, relevant to the calculation of the two-photon-exchange effects in atomic spectroscopy and electron scattering. We report on a complete next-to-leading-order (NLO) calculation of low-energy VVCS in chiral perturbation theory (χ PT). Here we focus on the unpolarized VVCS amplitudes $T_1(\nu, Q^2)$ and $T_2(\nu, Q^2)$, and the corresponding structure functions $F_1(x, Q^2)$ and $F_2(x, Q^2)$. Our results are confronted, where possible, with “data-driven” dispersive evaluations of low-energy structure quantities, such as nucleon polarizabilities. We find significant disagreements with dispersive evaluations at very low momentum-transfer Q ; for example, in the slope of polarizabilities at zero momentum-transfer. By expanding the results in powers of the inverse nucleon mass, we reproduce the known “heavy-baryon” expressions. This serves as a check of our calculation, as well as demonstrates the differences between the manifestly Lorentz-invariant ($B\chi$ PT) and heavy-baryon ($HB\chi$ PT) frameworks.

CONTENTS

I. Introduction and outline	3
II. VVCS formalism	4
III. Calculation of the VVCS amplitude at NLO	7
A. Remarks on power counting	7
B. Renormalization	11
C. Uncertainty estimate	11
IV. Results and discussion	12
A. $M_1^{(2)}(Q^2)$ — the generalized Baldin sum rule	12
B. $\alpha_L(Q^2)$ — the longitudinal polarizability	16
C. $M_2^{(1)}(Q^2)$ — the first moment of $F_2(x, Q^2)$	17
D. $M_1^{(4)}(Q^2)$ — the generalized fourth-order Baldin sum rule	19
E. $\bar{T}_1(\mathbf{0}, Q^2)$ — the proton subtraction function	20
V. Summary and conclusions	21
Acknowledgements	22
A. Photoabsorption cross sections	22
B. Polarizabilities at $Q^2 = 0$	25
1. πN -loop contribution	25
2. Δ -exchange contribution	27
References	28

I. INTRODUCTION AND OUTLINE

The forward doubly-virtual Compton scattering (VVCS), Fig. 1, is not a directly observable process. Nevertheless, it is traditionally of high relevance in studies of nucleon and nuclear structure, and of their impact on atomic nuclei. At high energies the VVCS has the apparent connections to deep-inelastic scattering, whereas at low energies it is important for precision atomic spectroscopy, where it serves as input for calculations of the nuclear-structure corrections. Analytical properties of the VVCS amplitude are used to establish useful relations — sum rules — between the static (electromagnetic moments, polarizabilities) and dynamic (photoabsorption cross sections) properties of the nucleon [1–5], see also Refs. [6–11] for reviews.

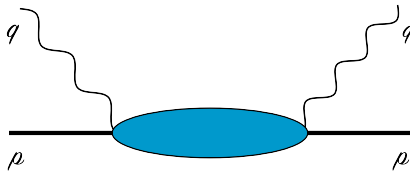


FIG. 1. The forward Compton scattering, or VVCS, in case of virtual photons, $q^2 = -Q^2$.

In the last decade, with the advent of muonic-atom spectroscopy by the CREMA Collaboration [12–14], the interest in nucleon VVCS has resurged in the context of the “proton radius puzzle” (see, e.g., Refs. [15, 16] for reviews). The muonic atoms, being more sensitive to nuclear structure than conventional atoms, demand a higher quality of this input in both the Lamb shift [12, 13] and, in the near future, the hyperfine structure measurements [17–19]. The VVCS enters here in the form of the two-photon exchange (TPE) corrections appearing at $\mathcal{O}(Z^4\alpha^5)$, which is the subleading order for the nuclear-structure effects in the Lamb shift (the leading being the charge radius), and leading in the hyperfine structure. In either case, the TPE is the leading theoretical uncertainty and precisising this contribution is a challenge for the nuclear and hadron physics community.

In this work we focus on the unpolarized nucleon VVCS, described, for each nucleon (proton or neutron), by two scalar amplitudes $T_{1,2}(\nu, Q^2)$, functions of the photon energy ν and virtuality Q^2 . The discontinuity of these amplitudes is given, respectively, by the two unpolarized structure functions $F_1(x, Q^2)$ and $F_2(x, Q^2)$.

To date, there are two approaches: 1) *dispersion relations (DR)* and 2) *chiral perturbation theory (χPT)*, used for evaluation of nucleon VVCS, with the goal of quantifying the relevant corrections in muonic hydrogen. It is expected and highly desirable that 3) *lattice QCD* will join this effort in the near future. In the mean time, however, the DR approach is the most popular one. It employs the well-known dispersion relations expressing the VVCS amplitudes as integrals of the structure functions known empirically from inclusive electron scattering.

Unfortunately, the DRs determine the VVCS in terms of the structure functions only up to a “subtraction function” $T_1(0, Q^2)$. The latter function is not well-constrained em-

pirically, which makes this approach prone to model uncertainties. It is worth to mention that there is a new proposal on how the subtraction can further be constrained via the dilepton electroproduction [20]. However, in the foreseeable future, this issue will preclude a systematic improvement of the theoretical uncertainty within the DR approach.

Here we employ the second approach. More specifically, we use an extension of SU(2) χ PT [21, 22] to the single-baryon sector [23–25], referred to as the baryon χ PT (B χ PT), augmented by inclusion of the explicit $\Delta(1232)$ -isobar in the δ -counting scheme [26]. In this framework we compute the inelastic (non-Born) part of the VVCS amplitudes to next-to-leading order (NLO). A first version of this calculation was briefly considered in Ref. [27]. Here we provide a few important improvements, in particular, the inclusion of the Coulomb-quadrupole ($C2$) $N \rightarrow \Delta$ transition, and a more comprehensive comparison of our results with the DR approach. The impact of this calculation on the muonic-hydrogen Lamb shift, extending our previous evaluation [28] to higher orders, will be discussed elsewhere.

The paper is organized as follows. In Sec. II, we recall the general formulae for VVCS and its relation to structure functions, form factors and polarizabilities. In Sec. III, we discuss the main ingredients of our NLO calculation. In Sec. IV, we examine results for the proton and neutron scalar polarizabilities, and some of the other moments of structure functions. In the concluding section (Sec. V), we summarize and give a brief outlook for the near-future work. In App. A, we discuss the structure functions, in particular, the πN , $\pi\Delta$ and Δ production channels relevant to our calculation. In App. B, we give analytical expressions for the πN -loop and Δ -exchange contributions to the static values and slopes of the polarizabilities and moments of structure functions. The complete expressions, also for the $\pi\Delta$ -loop contributions, can be found in the *Supplemented material*.

II. VVCS FORMALISM

Figure 1 schematically shows the VVCS amplitude, which for an unpolarized target (of any spin) can be decomposed into two independent Lorentz-covariant and gauge-invariant tensor structures [9]:

$$T^{\mu\nu}(p, q) = \left(-g^{\mu\nu} + \frac{q^\mu q^\nu}{q^2}\right) T_1(\nu, Q^2) + \frac{1}{M_N^2} \left(p^\mu - \frac{p \cdot q}{q^2} q^\mu\right) \left(p^\nu - \frac{p \cdot q}{q^2} q^\nu\right) T_2(\nu, Q^2), \quad (1)$$

where p and q are the four-momenta of the target particle and the photon, respectively; M_N is the target (here, nucleon) mass. The scalar amplitudes T_i are functions of the photon energy $\nu = p \cdot q/M_N$ and virtuality $Q^2 = -q^2$.

The optical theorem relates the absorptive parts of the VVCS amplitudes to the structure

functions, or equivalently, the inclusive electroproduction cross sections:

$$\begin{aligned}\text{Im } T_1(\nu, Q^2) &= \frac{4\pi^2\alpha}{M_N} F_1(x, Q^2) \\ &= K(\nu, Q^2) \sigma_T(\nu, Q^2),\end{aligned}\tag{2a}$$

$$\begin{aligned}\text{Im } T_2(\nu, Q^2) &= \frac{4\pi^2\alpha}{\nu} F_2(x, Q^2) \\ &= \frac{Q^2 K(\nu, Q^2)}{\nu^2 + Q^2} [\sigma_T(\nu, Q^2) + \sigma_L(\nu, Q^2)],\end{aligned}\tag{2b}$$

with the fine-structure constant $\alpha = e^2/4\pi$, and the Bjorken variable $x = Q^2/2M_N\nu$. The two response functions σ_T and σ_L are cross sections of total photoabsorption of transversely (T) and longitudinally (L) polarized photons. The flux of virtual photons is conventionally defined up to the flux factor $K(\nu, Q^2)$. The experimental observables do not depend on it, only the definitions of the response functions σ_T and σ_L do. Throughout this work we adopt Gilman's flux factor (for other common choices, cf. Ref. [6]):

$$K(\nu, Q^2) = |\vec{q}| = \sqrt{\nu^2 + Q^2},\tag{3}$$

where \vec{q} is the photon three-momentum in the lab frame.

The VVCS amplitudes satisfy the following dispersion relations derived from the above statement of the optical theorem, combined with general principles of analyticity and crossing symmetry (cf., for example, Refs. [6, 9, 10] for details):

$$\begin{aligned}T_1(\nu, Q^2) &= T_1(0, Q^2) + \frac{32\pi\alpha M_N \nu^2}{Q^4} \int_0^1 dx \frac{x F_1(x, Q^2)}{1 - x^2(\nu/\nu_{\text{el}})^2 - i0^+} \\ &= T_1(0, Q^2) + \frac{2\nu^2}{\pi} \int_{\nu_{\text{el}}}^\infty \frac{d\nu'}{\nu'} \frac{\sqrt{\nu'^2 + Q^2} \sigma_T(\nu', Q^2)}{\nu'^2 - \nu^2 - i0^+},\end{aligned}\tag{4a}$$

$$\begin{aligned}T_2(\nu, Q^2) &= \frac{16\pi\alpha M_N}{Q^2} \int_0^1 dx \frac{F_2(x, Q^2)}{1 - x^2(\nu/\nu_{\text{el}})^2 - i0^+} \\ &= \frac{2Q^2}{\pi} \int_{\nu_{\text{el}}}^\infty d\nu' \frac{\nu' [\sigma_T + \sigma_L](\nu', Q^2)}{\sqrt{\nu'^2 + Q^2}(\nu'^2 - \nu^2 - i0^+)},\end{aligned}\tag{4b}$$

with $\nu_{\text{el}} = Q^2/2M_N$ the elastic threshold. The high-energy behavior of $F_1(x, Q^2)$ prevents the convergence of the corresponding unsubtracted dispersion integral, hence leading to the once-subtracted dispersion relation, Eq. (4a), with the aforementioned ‘‘subtraction function’’ $T_1(0, Q^2)$. Note that while the subtraction point is conventionally chosen at $\nu = 0$, other choices are in principle possible. Future lattice QCD calculations of the VVCS amplitude would likely prefer to deal with a Euclidean subtraction point, e.g., at $\nu = iQ/2$, as chosen in Ref. [29].

The amplitudes are naturally split into nucleon-pole (T_i^{pole}) and non-pole (T_i^{nonpole}) parts, or Born (T_i^{Born}) and non-Born (\bar{T}_i) terms,

$$T_i = T_i^{\text{pole}} + T_i^{\text{nonpole}} = T_i^{\text{Born}} + \bar{T}_i,\tag{5}$$

with the pole and Born terms given uniquely in terms of the nucleon electric (G_E) and magnetic (G_M) Sachs form factors:

$$T_1^{\text{pole}}(\nu, Q^2) = \frac{4\pi\alpha}{M_N} \frac{\nu_{\text{el}}^2}{\nu_{\text{el}}^2 - \nu^2 - i0^+} G_M^2(Q^2), \quad (6a)$$

$$T_2^{\text{pole}}(\nu, Q^2) = \frac{8\pi\alpha\nu_{\text{el}}}{\nu_{\text{el}}^2 - \nu^2 - i0^+} \frac{G_E^2(Q^2) + \tau G_M^2(Q^2)}{1 + \tau}, \quad (6b)$$

$$T_1^{\text{Born}}(\nu, Q^2) = -\frac{4\pi\alpha}{M_N} \left[\frac{G_E(Q^2) + \tau G_M(Q^2)}{1 + \tau} \right]^2 + T_1^{\text{pole}}(\nu, Q^2), \quad (6c)$$

$$T_2^{\text{Born}}(\nu, Q^2) = T_2^{\text{pole}}(\nu, Q^2), \quad (6d)$$

where $\tau = Q^2/4M_N^2$. The $i0^+$ prescription represents the fact that the imaginary part of these amplitudes is given by the elastic piece of the structure functions: $F_i^{\text{el}}(Q^2) = F_i(x = 1, Q^2)$. One can thus exclude the pole piece from the above dispersion relations by setting the lower-energy limit of integration to an inelastic threshold ν_0 instead of ν_{el} , or $x_0 = Q^2/2M_N\nu_0$ instead of 1. For the nucleon the first inelastic threshold is usually associated with one-pion production, i.e., $\nu_0 = \nu_{\text{el}} + m_\pi(1 + m_\pi/2M_N)$, where m_π is the pion mass.

We are not concerned here with the elastic form factors, and therefore in the rest of the paper we focus on the non-Born part of the amplitudes, \bar{T}_i . The low-energy and low-momentum expansion of these amplitudes is given in terms of the static polarizabilities, e.g., for the lowest-order terms one obtains

$$\bar{T}_1(\nu, Q^2)/4\pi = \beta_{M1}Q^2 + (\alpha_{E1} + \beta_{M1})\nu^2 + \dots, \quad (7a)$$

$$\bar{T}_2(\nu, Q^2)/4\pi = (\alpha_{E1} + \beta_{M1})Q^2 + \dots, \quad (7b)$$

where α_{E1} (β_{M1}) is the electric (magnetic) dipole polarizability. Such an expansion of both sides of the dispersion relations (4) thus results in various sum rules, most notably, the Baldin sum rule [30] for $\alpha_{E1} + \beta_{M1}$. Further relations derived from unpolarized VVCS are considered in Ref. [31].

More generally, one may expand the dispersion relations (4) in ν alone, keeping Q^2 fixed. On the right hand side, one finds the moments of structure functions. Introducing

$$M_1^{(n)}(Q^2) \equiv \frac{4\alpha}{Q^2} \left(\frac{2M_N}{Q^2} \right)^{n-1} \int_0^{x_0} dx x^{n-1} F_1(x, Q^2), \quad (8a)$$

$$M_2^{(n)}(Q^2) \equiv \frac{4\alpha M_N}{Q^4} \left(\frac{2M_N}{Q^2} \right)^{n-1} \int_0^{x_0} dx x^{n-1} F_2(x, Q^2), \quad (8b)$$

the relations (4) lead to:

$$\bar{T}_1(\nu, Q^2) = \bar{T}_1(0, Q^2) + 4\pi \sum_{k=1} M_1^{(2k)}(Q^2) \nu^{2k}, \quad (9a)$$

$$\bar{T}_2(\nu, Q^2) = 4\pi \sum_{k=0} M_2^{(2k+1)}(Q^2) \nu^{2k}. \quad (9b)$$

Note that in the limit of $Q^2 \rightarrow 0$, we obtain the Baldin sum rule in the form:

$$\alpha_{E1} + \beta_{M1} = M_1^{(2)}(0) = M_2^{(1)}(0). \quad (10)$$

We refer to $M_1^{(2)}(Q^2)$ as the generalized Baldin sum rule, see Sec. IV A. More generally, we have the following relation (for an integer n):

$$M_1^{(n)}(0) = M_2^{(n-1)}(0), \quad (11)$$

arising from electromagnetic gauge invariance. One way to derive it is to introduce the longitudinal amplitude

$$T_L(\nu, Q^2) = -T_1(\nu, Q^2) + \frac{Q^2 + \nu^2}{Q^2} T_2(\nu, Q^2) \quad (12)$$

and to show that $\lim_{Q^2 \rightarrow 0} T_L(\nu, Q^2) = 0$. Incidentally, the same is true for asymptotically large Q^2 , because of the Callan-Gross relation: $2xF_1(x, Q^2) = F_2(x, Q^2)$, and hence $M_1^{(n)}(\infty) = M_2^{(n-1)}(\infty)$.

In what follows, we consider some of these moments, obtaining them from the χ PT results for the VVCS amplitudes, and compare them with the results of empirical parametrizations of the nucleon structure functions. The dispersion relations (4) are used by us to cross-check the results, using the tree-level photoabsorption cross sections discussed in App. A.

III. CALCULATION OF THE VVCS AMPLITUDE AT NLO

Our goal here is to obtain the χ PT predictions of the non-Born parts of the nucleon VVCS amplitudes $T_{1,2}$. The present NLO calculation is still within the “predictive powers” of χ PT for Compton scattering (CS) amplitudes, i.e., the results are given in terms of well-known parameters (see Table I) obtained from non-Compton processes. In this sense, it is complementary to the existing calculations of real CS (RCS) [32, 33], and the virtual CS (VCS) [34]. All of these studies, including the present one, are done in the same framework, using the same set of parameters.

A. Remarks on power counting

We shall employ B χ PT, which is the manifestly-covariant extension of χ PT to the single-baryon sector in its most straightforward implementation, where the nucleon is included as in Ref. [23]. The power-counting concerns raised in Ref. [23] have been overcome by renormalizing away the “power-counting violation” using the low-energy constants (LECs) available at that order. This has been shown explicitly within the “extended on-mass-shell renormalization scheme” (EOMS) [25], but is not limited to it. The inclusion of the explicit $\Delta(1232)$ here will follow the “ δ -counting” framework of Ref. [26] (see also Refs. [35, 36] for concise overviews).

To explain the power counting in more detail, let us recall that chiral effective-field theory is based on a perturbative expansion in powers of pion momentum p and mass m_π over the scale of spontaneous chiral symmetry breaking $\Lambda_\chi \sim 4\pi f_\pi$, with $f_\pi \simeq 92$ MeV the pion decay

constant. Each operator in the effective Lagrangian, or a graph in the loopwise expansion of the S -matrix, can have a specific order of p assigned to it.

To give a relevant example consider the following operator:

$$\mathcal{L}^{(4)} \sim \delta\beta \bar{N} N F^2, \quad (13)$$

with $\delta\beta$ the coupling constant, N the Dirac field of the nucleon, and F^2 the square of the electromagnetic field strength tensor, $F_{\mu\nu} = \partial_{[\mu} A_{\nu]}$. This is an operator of $\mathcal{O}(p^4)$. Two of the p 's come from the photon momenta which are supposed to be small, and the other two powers arise because the two-photon coupling to the nucleon must carry a factor of α (the charge e counts as p , since we want the derivative of the pion field to count as p even after including the minimal coupling to the photon).

This operator enters the effective Lagrangian with an LEC, which we denote $\delta\beta$. It gives a contribution to the CS amplitude in the form of¹

$$T^{\mu\nu} = 4\pi \delta\beta (q \cdot q' g^{\mu\nu} - q^\mu q'^\nu), \quad (14)$$

and leads to a shift in the magnetic dipole polarizability as: $\beta_{M1} \rightarrow \beta_{M1} + \delta\beta$. Now, two remarks are in order.

- i) *Naturalness*. The magnitude of the LEC is not arbitrary. It goes as $\delta\beta = (\alpha/\Lambda_\chi^3)c$, with the dimensionless constant c being of the order of 1, or more precisely:

$$p/\Lambda_\chi \ll |c| \ll \Lambda_\chi/p. \quad (15)$$

This condition ensures that the contribution of this operator is indeed of $\mathcal{O}(p^4)$, as inferred by the power counting.

- ii) *Predictive powers*. This LEC enters very prominently in the polarizabilities and CS at tree level, which means its value is best fixed by the empirical information on these quantities. If this is so, the $\mathcal{O}(p^4)$ result is not “predictive”, as it could only be used to *fit* the χ PT expression to experiment or lattice QCD calculations. On the other hand, contributions of orders lower than p^4 are predictive, as they only contain LECs fixed from elsewhere.

As already mentioned, the “predictive” contributions to CS and polarizabilities have been identified and computed for the case of RCS [32], VCS [34], and VVCS [27]. Our present calculation is quite analogous to those works and hence we refer to them for most of the technical details, such as the expressions for the relevant terms of the effective Lagrangian. It is crucial to first study these predictive contributions. We note, however, that here we choose to also include the p^4 LEC that shifts the magnetic polarizability. In doing so, we fit the value of $\delta\beta$ so as to reproduce the Baldin sum rule values:

$$\alpha_{E1p} + \beta_{M1p} = 14.0(0.2) \times 10^{-4} \text{ fm}^3 \quad \text{proton [37]} \quad (16a)$$

$$\alpha_{E1n} + \beta_{M1n} = 15.2(0.5) \times 10^{-4} \text{ fm}^3 \quad \text{neutron [38]}, \quad (16b)$$

¹ Throughout this paper we use the conventions summarized in the beginning of Ref. [9].

taking the values of α_{E1} obtained at $\mathcal{O}(p^4/\Delta)$ as B χ PT predictions. This choice reflects the fact that the most prominent scalar moments considered here, the second moment of $F_1(x, Q^2)$ and the first moment of $F_2(x, Q^2)$, both have the Baldin sum rule as their static limit. The values of the magnetic polarizabilities that result from this fit are

$$\beta_{M1p} = 2.75(0.2) \times 10^{-4} \text{ fm}^3, \quad \beta_{M1n} = 1.5(0.5) \times 10^{-4} \text{ fm}^3, \quad (17)$$

where the error bar does not include the theoretical uncertainty. One has to admit that this procedure results in somewhat smaller values of β_{M1} than, for instance, those obtained in the recent HB and covariant chiral analyses: $3.2(0.5) \times 10^{-4} \text{ fm}^3$ [39, 40] for the proton and $3.65(1.25) \times 10^{-4} \text{ fm}^3$ [41] for the neutron. We will, however, use this simplified procedure since the only affected quantity studied by us is the proton subtraction function $\bar{T}_{1p}(0, Q^2)/4\pi = \beta_{M1p} Q^2 + \dots$, and the discrepancy for β_{M1p} is tolerable.



FIG. 2. Tree-level $\Delta(1232)$ -exchange diagram.

We also include the Coulomb-quadrupole ($C2$) $N \rightarrow \Delta$ transition, described by the g_C term in the following non-minimal $\gamma^* N \Delta$ coupling [42, 43] (note that in these references the overall sign of g_C is inconsistent between the Lagrangian and Feynman rules):

$$\begin{aligned} \mathcal{L}_\Delta^{(2)} = & \frac{3e}{2M_N M_+} \bar{N} T_3 \left\{ i g_M \tilde{F}^{\mu\nu} \partial_\mu \Delta_\nu - g_E \gamma_5 F^{\mu\nu} \partial_\mu \Delta_\nu \right. \\ & \left. + i \frac{g_C}{M_\Delta} \gamma_5 \gamma^\alpha (\partial_\alpha \Delta_\nu - \partial_\nu \Delta_\alpha) \partial_\mu F^{\mu\nu} \right\} + \text{H.c.}, \end{aligned} \quad (18)$$

with $M_+ = M_N + M_\Delta$ and the dual of the electromagnetic field strength tensor $\tilde{F}^{\mu\nu} = \frac{1}{2} \epsilon^{\mu\nu\rho\lambda} F_{\rho\lambda}$. The electric, magnetic and Coulomb couplings (g_E , g_M and g_C) are known from the analysis of pion photoproduction P_{33} multipoles [43]. The corresponding numerical values, as well as those of other physical constants used in this work, are given in Table I. The Coulomb coupling is subleading compared with the electric and magnetic couplings, and it was not included in the previous calculations. However, the relatively large magnitude of g_C hints at its potential numerical importance, which we examine in this work.

The counting of the $\Delta(1232)$ effects is done within “ δ -counting” [26], where the Delta-nucleon mass difference, $\Delta = M_\Delta - M$, is a light scale ($\Delta \ll \Lambda_\chi$) which is substantially heavier than the pion mass ($m_\pi \ll \Delta$). Hence, if $p \sim m_\pi$, then $\mathcal{O}(p^4/\Delta)$ is in between of $\mathcal{O}(p^3)$ and $\mathcal{O}(p^4)$.

For the non-Born VVCS amplitudes and polarizabilities the predictive orders are $\mathcal{O}(p^3)$ and $\mathcal{O}(p^4/\Delta)$. The $\mathcal{O}(p^3)$ contribution comes from the pion-nucleon (πN) loops. We refer to it here as the LO contribution.² The $\mathcal{O}(p^4/\Delta)$ contribution, arising at the NLO, comes

² In the full Compton amplitude, there is a lower order contribution coming from the Born terms, leading to a shift in nomenclature by one order: the LO contribution referred to as the NLO contribution, etc., see e.g. Ref. [32].

from the tree-level Delta-exchange (Δ -exchange) graph shown in Fig. 2, and the pion-Delta ($\pi\Delta$) loops. The loop diagrams are shown in Ref. [27, Figs. 1 and 2].

The Δ -exchange graph is described by the $\gamma^*N\Delta$ interaction in Eq. (18). For the magnetic coupling, one assumes a dipole behavior to mimic the form expected from vector-meson dominance:

$$g_M \rightarrow \frac{g_M}{[1 + (Q/\Lambda)^2]^2}, \quad (19)$$

with the dipole mass $\Lambda^2 = 0.71 \text{ GeV}^2$. The inclusion of this Q^2 dependence is motivated by observing the importance of this form factor for the correct description of the electroproduction data [42]. Since electroproduction off the nucleon is directly connected with the nucleon polarizabilities via sum rules, it is understandable that a better description of the electroproduction data will lead to a better description of the Q^2 behavior of the polarizabilities. The effect of the dipole form factor in g_M is illustrated in Figs. 4, 6, and 7.

A feature of the δ -counting is that the characteristic momentum p distinguishes two regimes: the *low-energy* ($p \simeq m_\pi$) and *resonance* ($p \simeq \Delta$) regimes. The above counting is limited to the low-energy regime. Since we are interested in the low-energy expansion of the VVCS amplitudes (i.e., the expansion in powers of small ν with Q^2 finite), we do not consider the regime where one-Delta-reducible graphs are enhanced (resonance regime). However, going to higher Q^2 one does need to count the Delta propagators similar to the nucleon propagators, which, in turn, calls for inclusion of $\pi\Delta$ loops with two and three Delta propagators, which have been omitted here. They are only included implicitly by adjusting the isospin coefficients of the one-nucleon-reducible $\pi\Delta$ -loop graphs to restore current conservation, as explained in the next section. Apart from that, $\pi\Delta$ loops have a rather mild dependence on momenta and the missing loops are unlikely to affect the Q^2 -dependence of the moments of structure functions significantly, even for Q^2 comparable to Δ^2 .

TABLE I. Parameters (fundamental and low-energy constants) [44] at the order they first appear. The $\pi N\Delta$ coupling constant h_A is fit to the experimental Delta width and the $\gamma^*N\Delta$ coupling constants g_M , g_E and g_C are taken from the pion photoproduction study of Ref. [42]. The free parameters $\delta\beta_{p,n}$ are fitted to the Baldin sum rule for the proton and neutron [37, 38], respectively.

$\mathcal{O}(p^2)$	$\alpha \simeq 1/(137.04)$, $M_N = M_p \simeq 938.27 \text{ MeV}$
$\mathcal{O}(p^3)$	$g_A \simeq 1.27$, $f_\pi \simeq 92.21 \text{ MeV}$, $m_\pi \simeq 139.57 \text{ MeV}$
$\mathcal{O}(p^4/\Delta)$	$M_\Delta \simeq 1232 \text{ MeV}$, $h_A \equiv 2g_{\pi N\Delta} \simeq 2.85$, $g_M \simeq 2.97$, $g_E \simeq -1.0$, $g_C \simeq -2.6$
$\mathcal{O}(p^4)$	$\delta\beta_p = -1.12 \times 10^{-4} \text{ fm}^3$, $\delta\beta_n = -3.10 \times 10^{-4} \text{ fm}^3$

B. Renormalization

The calculation of the πN - and $\pi\Delta$ -loop graphs is analogous to Ref. [32], with the obvious extension to the case of a finite photon virtuality. The renormalization is also done in the exact same way; namely, subtracting the loop contribution to the Born term of the the VVCS amplitude. The $\pi\Delta$ -loop graphs still contain divergences after this subtraction. These divergences are of higher orders, $\mathcal{O}(p^5/\Delta^2)$ and $\mathcal{O}(p^4)$, and will be cancelled by the corresponding higher-order contact terms. In practice, they are removed by taking the $\overline{\text{MS}}$ values of the divergent quantities.

As mentioned above, $\pi\Delta$ -loop graphs where photons couple minimally to the Delta contain more than one Delta propagator and therefore should be suppressed by extra powers of p/Δ . However, their lower-order contributions are important for electromagnetic gauge invariance and therefore for the renormalization procedure. In particular, the lower-order contributions of chiral loops should not affect the result of the low-energy theorem [45, 46], and this condition is automatically satisfied by a subset of graphs if it obeys gauge invariance. The $\pi\Delta$ -loop graphs, cf. Ref. [27, Fig. 2], form such a subset for the case of the neutral Delta. In reality, the Delta comes in four charge states (isospin 3/2), thus, a gauge-invariant set will in addition have the higher-order graphs where the photon couples minimally to the Delta. To make the subset of $\pi\Delta$ -loop graphs gauge invariant without the higher-order graphs, we used the same procedure as in Ref. [32]. The one-particle-irreducible (1PI) graphs in Ref. [27, Fig. 2] are computed with the correct isospin factors, i.e., summing over all charge states of the Delta, whereas the isospin factors for the one-particle-reducible (1PR) loop graphs are chosen such that their ratio to the isospin factors of 1PI graphs is the same as in the neutral Delta case. This procedure automatically ensures exact gauge invariance and thus effectively includes the relevant contributions of the one-loop graphs with minimal coupling of photons to the Delta. If the latter graphs are included explicitly, the isospin factors of 1PR graphs can be restored to actual values. The corresponding change in the values of the polarizabilities, however, is of higher order than what we consider in this work.

C. Uncertainty estimate

To estimate the uncertainties of our NLO predictions, we define the running expansion parameter

$$\tilde{\delta}(Q^2) = \sqrt{\left(\frac{\Delta}{M_N}\right)^2 + \left(\frac{Q^2}{2M_N\Delta}\right)^2}, \quad (20)$$

such that the N²LO is expected to be of relative size $\tilde{\delta}^2$ [42]. To estimate the uncertainty of a polarizability $P(Q^2)$ due to the neglected higher-order terms in the chiral expansion, we separate that polarizability into the static piece $P(0)$ and the Q^2 -dependent remainder $P(Q^2) - P(0)$. The uncertainty of $P(Q^2)$ is obtained by adding the estimates for these two

parts in quadrature:

$$\Delta P(Q^2) = \sqrt{\tilde{\delta}^4(0)P(0)^2 + \tilde{\delta}^4(Q^2)[P(Q^2) - P(0)]^2}, \quad (21)$$

The uncertainties in the values of the parameters have a much smaller impact compared to the truncation uncertainty and are therefore neglected.

IV. RESULTS AND DISCUSSION

We now consider the numerical results for some of the moments of the nucleon structure functions which appear in the expansion Eq. (9). We shall also consider the proton subtraction function $\bar{T}_1(0, Q^2)$. The complete NLO values will be decomposed into three individual contributions: the πN loops, the Δ exchange, and the $\pi\Delta$ loops. In practice, we extract all results from the calculated non-Born VVCS amplitudes. For a cross-check, we used the photoabsorption cross sections described in App. A.

A. $M_1^{(2)}(Q^2)$ — the generalized Baldin sum rule

The electric and magnetic dipole polarizabilities, $\alpha_{E1}(Q^2)$ and $\beta_{M1}(Q^2)$, encode information about the dipole response of the nucleon to an electromagnetic field. For finite momentum transfers, the sum of dipole polarizabilities is given by the generalized Baldin sum rule:

$$[\alpha_{E1} + \beta_{M1}](Q^2) = \frac{1}{2\pi^2} \int_{\nu_0}^{\infty} d\nu \sqrt{1 + \frac{Q^2}{\nu^2}} \frac{\sigma_T(\nu, Q^2)}{\nu^2} = \frac{8\alpha M_N}{Q^4} \int_0^{x_0} dx x F_1(x, Q^2), \quad (22)$$

where ν_0 is the lowest inelastic threshold, in this case the one-pion production threshold $\nu_0 = m_\pi + (m_\pi^2 + Q^2)/2M_N$, and $x_0 = Q^2/2M_N\nu_0$. The electric and magnetic dipole polarizabilities of the nucleon enter the nucleon-structure contributions to the Lamb shift of muonic hydrogen and other muonic atoms [28, 52–54], and thus are of major interest for an accurate extraction of the nuclear charge radii.

Our B χ PT predictions for $\alpha_{E1} + \beta_{M1}$ are shown in Fig. 3 {upper panel}, both for the proton and the neutron, up to photon virtualities of 0.3 GeV². Our main result is given by the blue solid lines and the blue error bands, where we used the p^4 LEC $\delta\beta$ to fit the static polarizabilities to the empirical Baldin sum rule values (green and purple dots) given in Eq. (16), see discussion in Sec. III A. Inclusion of $\delta\beta$, cf. Table I, merely leads to a constant shift, as can be seen by comparing to the pure $\mathcal{O}(p^4/\Delta)$ predictions (blue long-dashed lines), which include the πN -loop, the Δ -exchange and the $\pi\Delta$ -loop contributions. In order to illustrate the effect of the Delta in these predictions, we also plot the LO πN -loop contributions separately (red solid lines). We compare our results for the Q^2 evolution with the LO HB χ PT predictions [47] (purple dashed lines) and the MAID model predictions [48, 49] (black dotted lines). The latter are based on the generalized Baldin sum rule (22)

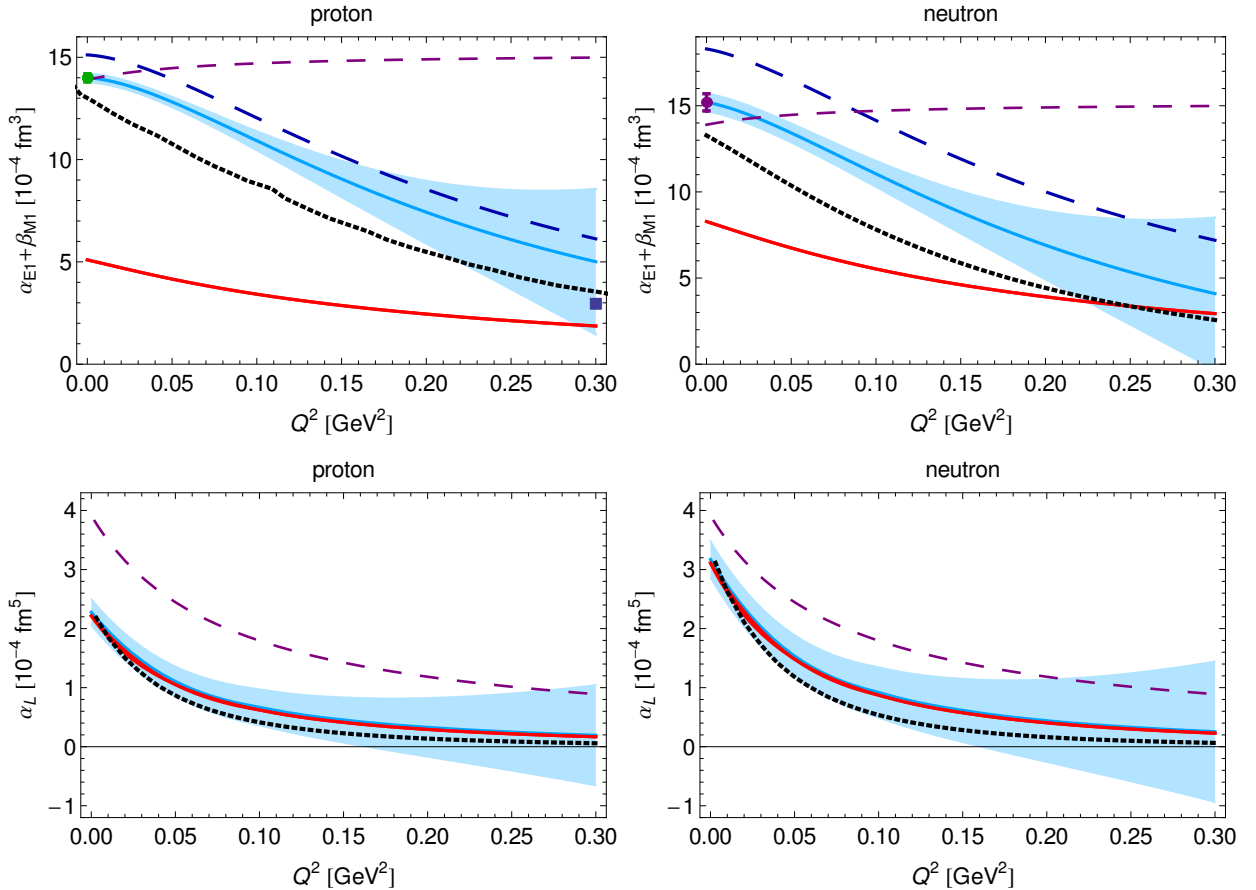


FIG. 3. Upper panel: Generalized Baldin sum rule for the proton (left) and neutron (right) as function of Q^2 . The result of this work, including the $\delta\beta$ contribution, is shown by the blue solid line, with the blue band representing the uncertainty due to higher-order effects. The blue long-dashed line shows the NLO $B\chi\text{PT}$ prediction (i.e., without the $\delta\beta$ term). The red line represents the LO $B\chi\text{PT}$ result, while the purple dashed line is the LO HB limit [47]. The black dotted line is the MAID model prediction [48–50]; for the proton we use the updated estimate from Ref. [6] that includes the $\pi, \eta, \pi\pi$ channels. At $Q^2 = 0 \text{ GeV}^2$, we show the Baldin sum rule value for the proton (green dot) [37] and neutron (purple dot) [38]. For the proton, the $Q^2 = 0.3 \text{ GeV}^2$ point (blue square) is the empirical evaluation of Ref. [51]. Lower panel: Longitudinal polarizability for the proton (left) and neutron (right). The NLO $B\chi\text{PT}$ predictions of this work are shown by the blue solid line with blue band; the legend for the remaining curves is as in the upper panel. Note that the LO $B\chi\text{PT}$ curves are practically on top of the NLO ones.

evaluated with $(\pi + \eta + \pi\pi)$ photoproduction cross sections [6]. The data points are also evaluations of the (generalized) Baldin sum rule [37, 51, 55]. One can see that the $B\chi\text{PT}$ predictions seem to systematically overestimate the MAID model in the Q^2 range shown here. One has to note that the MAID model, on the other hand, slightly underestimates the empirical Baldin sum rule evaluations.

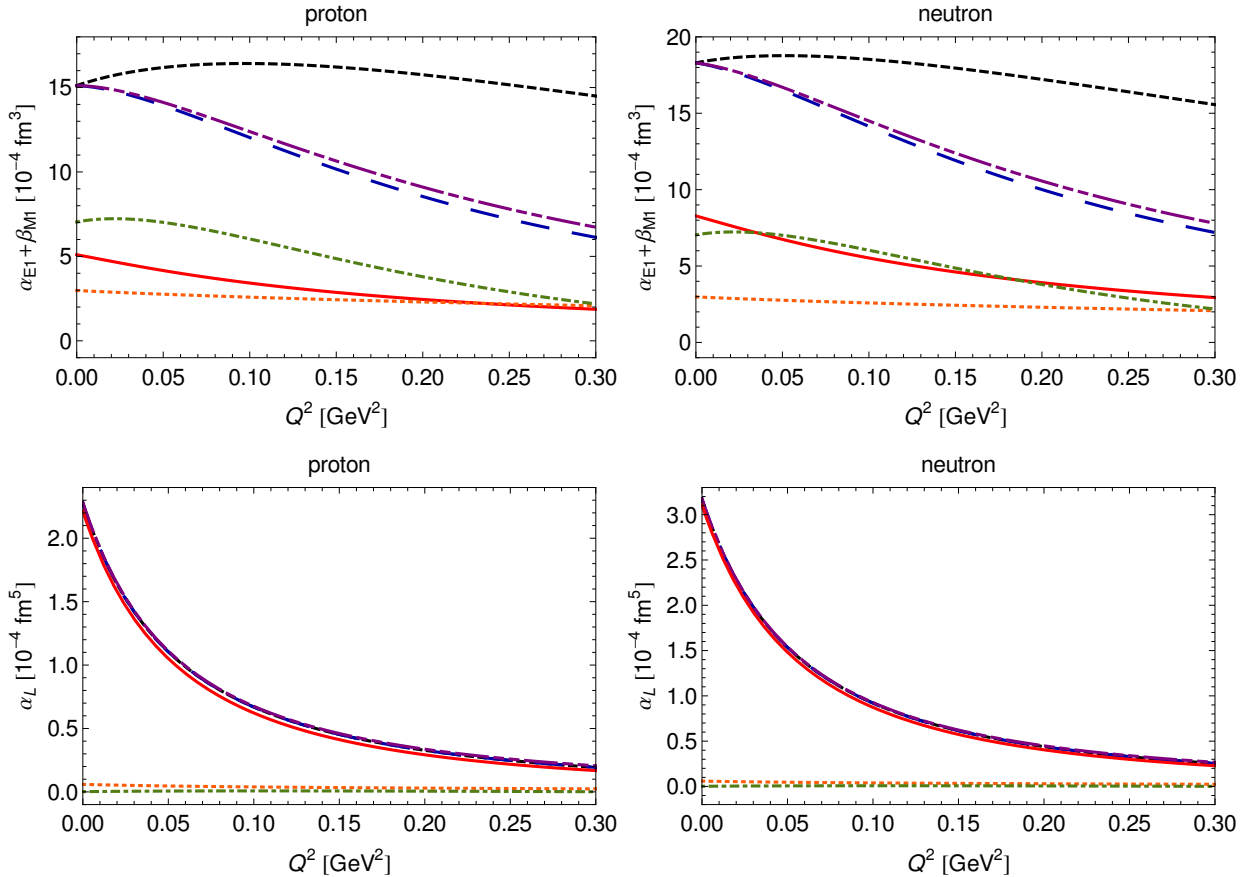


FIG. 4. Contributions of the different orders to the chiral predictions of $[\alpha_{E1} + \beta_{M1}](Q^2)$ {upper panel} and $\alpha_L(Q^2)$ {lower panel} for the proton (left) and neutron (right). Red solid line: πN -loop contribution, green dot-dashed line: Δ -exchange contribution, orange dotted line: $\pi\Delta$ -loop contribution, blue long-dashed line: total result, purple dot-dot-dashed line: total result without g_C contribution, black short-dashed line: total result without g_M dipole.

The LO HB results seem to agree with the empirical values at the real-photon point [55] both for the proton and the neutron. However, they do not fall off with increasing Q^2 in contrast to the $B\chi$ PT predictions. This asymptotic behavior is the reason for the large proton-polarizability effect on the muonic-hydrogen Lamb shift found within $HB\chi$ PT [47, 56, 57], much larger than the phenomenological value. As shown in Ref. [28, 31], this issue is solved within the relativistic formulation, which gives a result closer to calculations based on the dispersive approach.

The static dipole polarizabilities α_{E1} and β_{M1} have been studied within both the HB and the $B\chi$ PT. While $HB\chi$ PT gives results remarkably close to the experimental determinations already at LO [58], the contribution of the $\Delta(1232)$ is harder to accommodate in this framework [59]. In contrast to that, LO $B\chi$ PT [60, 61] yields smaller values for the sum of dipole polarizabilities, in disagreement with the empirically extracted values based on evaluations of the Baldin sum rule with modern photoabsorption data [37, 55, 62]. However, the NLO

contributions from Δ exchange and $\pi\Delta$ loops improve the situation [32, 33]. In the case of the proton, they bring the $B\chi$ PT result in agreement with the experimental extraction, while for the neutron the total result is slightly bigger. The $\Delta(1232)$ contributions are, therefore, naturally accommodated in $B\chi$ PT, and not in $HB\chi$ PT (where they can be reconciled with the empirical values only by means of the p^4 LEC $\delta\beta$, see, e.g., Refs. [40, 63] for the recent calculations and review).

The $B\chi$ PT contributions from πN loops, Δ exchange and $\pi\Delta$ loops to the static polarizabilities are, in that order and in the usual units of 10^{-4} fm^3 :

$$\alpha_{E1p} + \beta_{M1p} = 15.12(1.48) \approx 5.10 + 7.04 + 2.98, \quad (23a)$$

$$\alpha_{E1n} + \beta_{M1n} = 18.30(1.79) \approx 8.28 + 7.04 + 2.98. \quad (23b)$$

This NLO result is a prediction of $B\chi$ PT, i.e., it does not include the p^4 LEC $\delta\beta$ discussed in Sec. III A. The corresponding individual contributions to the Q^2 -dependent generalized polarizabilities are shown in Fig. 4 {upper panel}. For the proton, the dominant contribution in the studied Q^2 range is that of the Δ exchange, while for the neutron the πN -loop and Δ -exchange contributions are of roughly the same size. The importance of the Delta is related to the fact that the nucleon-to-Delta transition is dominantly of the magnetic dipole type, therefore it gives a huge contribution to β_{M1} .

In addition to the static values, we can now investigate the slopes of the polarizabilities at the real-photon point. Decomposing the results as before into the three contributions, we observe that $B\chi$ PT predicts large contributions to the slopes both from πN loops and Δ exchange. The Q^2 dependence generated by $\pi\Delta$ loops, on the other hand, is negligible, as can be clearly seen from Fig. 4. The numerical values for the individual contributions to the slopes are, in units of 10^{-4} fm^5 :

$$\left. \frac{d(\alpha_{E1p} + \beta_{M1p})(Q^2)}{dQ^2} \right|_{Q^2=0} = -0.19(6) \approx -0.74 + 0.74 - 0.20, \quad (24a)$$

$$\left. \frac{d(\alpha_{E1n} + \beta_{M1n})(Q^2)}{dQ^2} \right|_{Q^2=0} = -0.68(21) \approx -1.22 + 0.74 - 0.20. \quad (24b)$$

The dipole form factor in the magnetic coupling g_M generates the Q^2 fall-off of the dipole polarizabilities, cf. Fig. 4, which is also observed in parametrizations of experimental cross sections [64]. Due to cancellations between the πN -loop and the Δ -exchange contributions, the dipole also crucially affects the overall sign of the slope, as can be seen in Fig. 4. Note that due to these cancellations we estimate the relative error of the slope by $\tilde{\delta}$ instead of $\tilde{\delta}^2$.

Evaluating the Baldin sum rule radius,

$$r_{(\alpha+\beta)}^2 \equiv -\frac{6}{\alpha_{E1} + \beta_{M1}} \left. \frac{d}{dQ^2} [\alpha_{E1} + \beta_{M1}](Q^2) \right|_{Q^2=0}, \quad (25)$$

we obtain $r_{(\alpha+\beta)p} = 0.29(9) \text{ fm}$ and $r_{(\alpha+\beta)n} = 0.52(16) \text{ fm}$, where we estimated the relative error to be $\tilde{\delta}$. Here, we again used our result including the $\delta\beta$ contribution, i.e., we fixed

the static polarizabilities to the Baldin sum-rule values in Eq. (16), while the slope is still a prediction of B χ PT.

The result for the proton is in tension with the sum-rule evaluations [51, 64, 65] which use empirical parametrizations of the structure function $F_1(x, Q^2)$, e.g. [64]:

$$r_{(\alpha+\beta)p} = 0.98(5) \text{ fm.} \quad (26)$$

From Fig. 3 one can see that the MAID empirical parametrization also leads to a steeper slope than B χ PT. This calls for a careful revision of the low-momentum behavior of the empirical parametrizations in the near future.

B. $\alpha_L(Q^2)$ — the longitudinal polarizability

The low-energy expansion of the longitudinal VVCS amplitude goes as

$$T_L(\nu, Q^2)/4\pi = \alpha_{E1}Q^2 + \alpha_L Q^2 \nu^2 + \dots \quad (27)$$

with α_L called the longitudinal polarizability. Note that, in terms of the moments $\alpha_L = M_2^{(1)'}(0) - M_1^{(2)'}(0) + M_1^{(4)}(0)$. The generalized longitudinal polarizability is given by,

$$\alpha_L(Q^2) = \frac{1}{2\pi^2} \int_{\nu_0}^{\infty} d\nu \sqrt{1 + \frac{Q^2}{\nu^2}} \frac{\sigma_L(\nu, Q^2)}{Q^2 \nu^2} = \frac{4\alpha M_N}{Q^6} \int_0^{x_0} dx F_L(x, Q^2), \quad (28)$$

with

$$F_L(x, Q^2) = -2xF_1(x, Q^2) + \left(1 + \frac{4M_N^2 x^2}{Q^2}\right) F_2(x, Q^2).$$

Our B χ PT prediction for $\alpha_L(Q^2)$ is shown in Fig. 3 {lower panel}, where we compare our results, with and without the Delta contributions, with the MAID model predictions [6, 48–50] and the HB limit of the πN -loop contribution. One can see that the Delta plays a negligible role in the low- Q^2 evolution of α_L , which in the B χ PT approach is dominated by πN loops. Our results run very close to the MAID curves, with small discrepancies in the intermediate Q^2 region. At higher virtualities, these discrepancies decrease. The HB approach, on the other hand, seems to systematically overestimate the value of α_L in the considered Q^2 range. This relatively big mismatch can be traced back to the slow convergence of the $1/M_N$ expansion, as one can see from the analytic expression for the πN -loop contribution to $\alpha_L(Q^2 = 0)$ given in App. B.

For the static values of α_L , we obtain the following contributions from πN loops, Δ exchange and $\pi\Delta$ loops, in units of 10^{-4} fm^5 :

$$\alpha_{Lp} = 2.28(22) \approx 2.22 + 0.00 + 0.06, \quad (29a)$$

$$\alpha_{Ln} = 3.17(31) \approx 3.11 + 0.00 + 0.06. \quad (29b)$$

For the slopes at $Q^2 = 0$, we find, in units of 10^{-4} fm^7 :

$$\left. \frac{d\alpha_{Lp}(Q^2)}{dQ^2} \right|_{Q^2=0} = -1.63(16) \approx -1.62 + 0.01 - 0.01, \quad (30a)$$

$$\left. \frac{d\alpha_{Ln}(Q^2)}{dQ^2} \right|_{Q^2=0} = -2.25(22) \approx -2.24 + 0.01 - 0.01. \quad (30b)$$

The corresponding individual contributions to the Q^2 dependence of $\alpha_L(Q^2)$ are demonstrated in Fig. 4 {lower panel}. One again notices that Δ exchange and $\pi\Delta$ loops give negligible contributions in this Q^2 range. The smallness of the Δ -exchange contribution is explained by the fact that the magnetic coupling g_M does not contribute to α_L .

C. $M_2^{(1)}(Q^2)$ — the first moment of $F_2(x, Q^2)$

At $Q^2 = 0$, the first moment of the structure function $F_2(x, Q^2)$,

$$\begin{aligned} M_2^{(1)}(Q^2) &= \frac{1}{2\pi^2} \int_{\nu_0}^{\infty} \frac{d\nu}{\nu} \frac{1}{\sqrt{\nu^2 + Q^2}} \left[\sigma_T(\nu, Q^2) + \sigma_L(\nu, Q^2) \right], \\ &= \frac{4\alpha M_N}{Q^4} \int_0^{x_0} dx F_2(x, Q^2), \end{aligned} \quad (31)$$

reproduces the Baldin sum rule: $M_2^{(1)}(0) = \alpha_{E1} + \beta_{M1} = M_1^{(2)}(0)$, cf. Eq. (23). However, at finite Q^2 this moment is independent of $M_1^{(2)}(Q^2)$. Comparing Fig. 5 {upper panel}, which shows the Q^2 dependence of $M_2^{(1)}$, with the respective figure for $M_1^{(2)}$, Fig. 3 {upper panel}, one can indeed see that the two moments noticeably diverge as one departs from the static limit. Note that the contribution of the p^4 operator in Eq. (14) simultaneously shifts $M_1^{(2)}(0)$ and $M_2^{(1)}(0)$ so they both coincide with the empirical Baldin sum rule value. For the slope of $M_2^{(1)}$ at $Q^2 = 0$, we find the following contributions from πN loops, Δ exchange and $\pi\Delta$ loops, in units of 10^{-4} fm^5 :

$$\left. \frac{dM_{2p}^{(1)}(Q^2)}{dQ^2} \right|_{Q^2=0} = -3.92(38) \approx -1.47 - 2.18 - 0.26, \quad (32a)$$

$$\left. \frac{dM_{2n}^{(1)}(Q^2)}{dQ^2} \right|_{Q^2=0} = -4.81(47) \approx -2.37 - 2.18 - 0.26. \quad (32b)$$

Interestingly, the slope does not show such a drastic cancellation between the πN -loop and the Δ -exchange contribution as one encounters in the generalized Baldin sum rule. Correspondingly, the shape of the $M_2^{(1)}$ curve is not so much affected by the inclusion of the g_M dipole form factor, as one can see from Fig. 6 {upper panel} which shows the individual contributions to the Q^2 dependence of $M_2^{(1)}(Q^2)$.

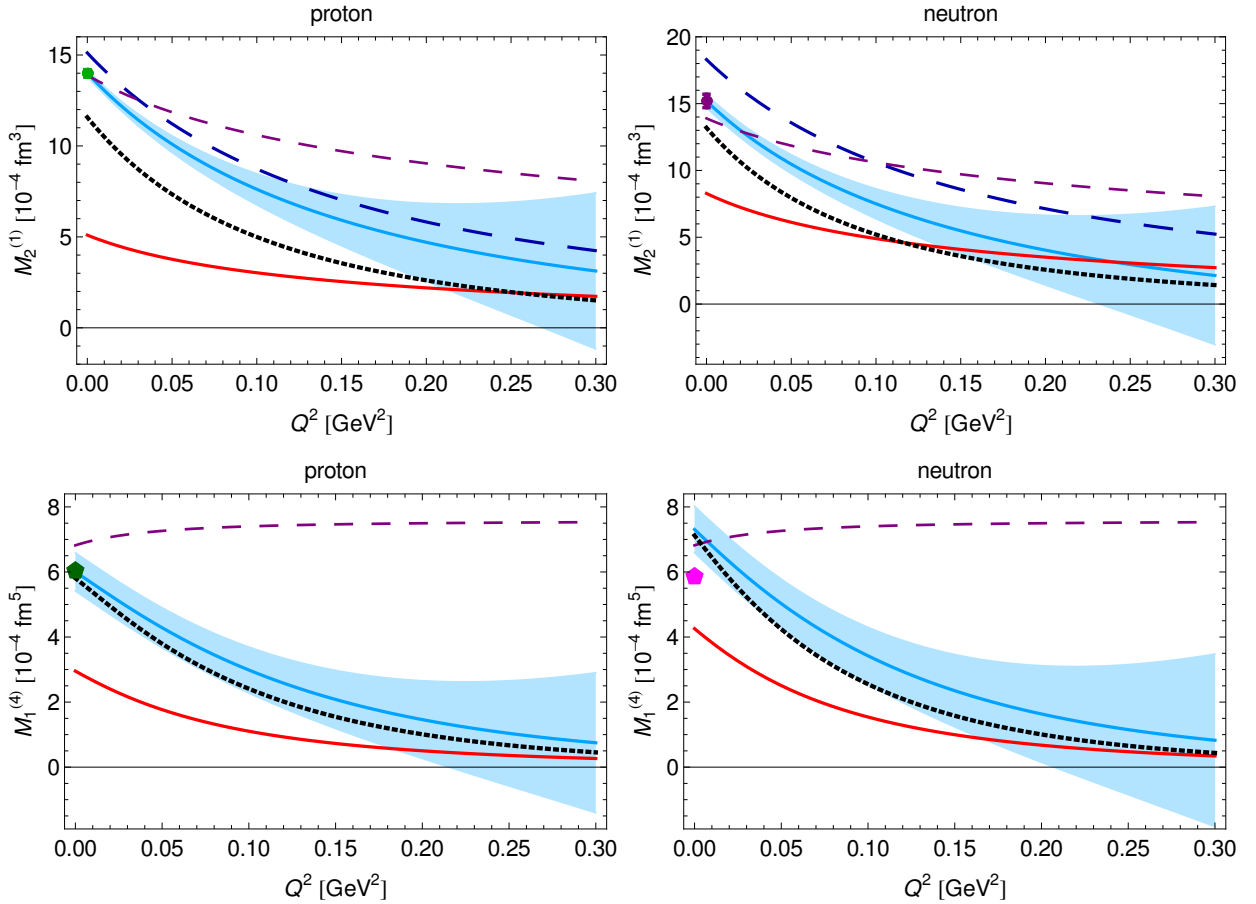


FIG. 5. Upper panel: The first moment of the structure function $F_2(x, Q^2)$ for the proton (left) and neutron (right) as function of Q^2 . The result of this work, including the $\delta\beta$ contribution, is shown by the blue solid line, with the blue band representing the uncertainty due to higher-order effects. The blue long-dashed line shows the NLO B χ PT prediction (i.e., without the $\delta\beta$ term). The red line represents the LO B χ PT result, while the purple dashed line is the LO HB limit [47]. The black dotted line is the MAID model prediction [48–50]. At $Q^2 = 0$ GeV², we show Baldin sum rule evaluations for the proton (green dot) [37] and neutron (purple dot) [38]. Lower panel: Fourth-order generalized Baldin sum rule for the proton (left) and neutron (right). The NLO B χ PT prediction of this work is shown by the blue solid line and the blue band; the legend for the remaining curves is as in the upper panel. At $Q^2 = 0$ GeV², we show fourth-order Baldin sum rule evaluations for the proton (dark green pentagon) [37] and neutron (magenta pentagon) [66].

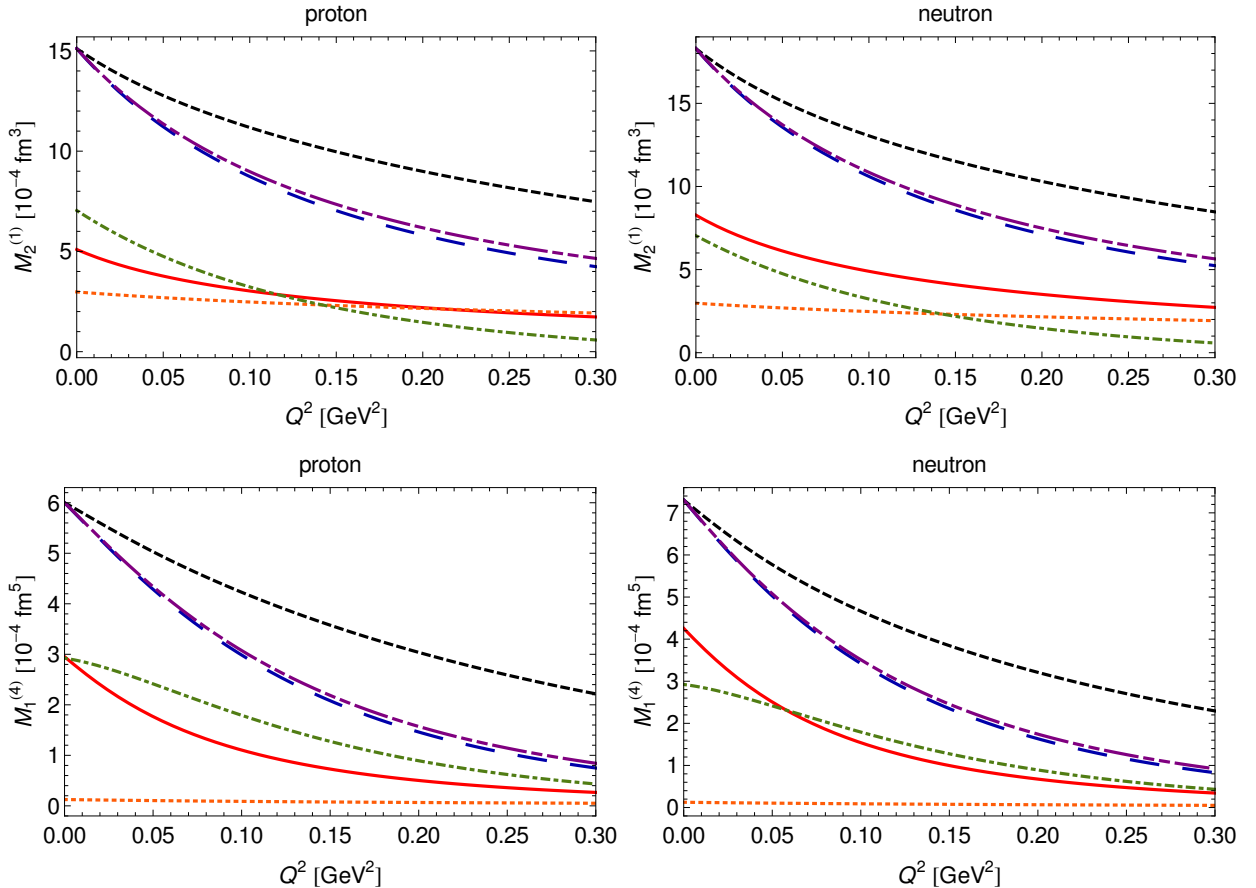


FIG. 6. Contributions of the different orders to the chiral prediction of $M_2^{(1)}(Q^2)$ {upper panel} and $M_1^{(4)}(Q^2)$ {lower panel} for the proton (left) and neutron (right). Red solid line: πN -loop contribution, green dot-dashed line: Δ -exchange contribution, orange dotted line: $\pi\Delta$ -loop contribution, blue long-dashed line: total result, purple dot-dot-dashed line: total result without g_C contribution, black short-dashed line: total result without g_M dipole.

D. $M_1^{(4)}(Q^2)$ — the generalized fourth-order Baldin sum rule

Let us now consider the fourth moment of the structure function $F_1(x, Q^2)$:

$$\begin{aligned}
 M_1^{(4)}(Q^2) &= \frac{1}{2\pi^2} \int_{\nu_0}^{\infty} d\nu \sqrt{1 + \frac{Q^2}{\nu^2}} \frac{\sigma_T(\nu)}{\nu^4} \\
 &= \frac{32\alpha M_N^3}{Q^8} \int_0^{x_0} dx x^3 F_1(x, Q^2).
 \end{aligned}
 \tag{33}$$

In the real-photon limit, this moment is related to a linear combination of dispersive and quadrupole polarizabilities [67, 68], resulting in the fourth-order Baldin sum rule (see Ref. [9] for review):

$$M_1^{(4)}(0) = \alpha_{E1\nu} + \beta_{M1\nu} + \frac{1}{12}(\alpha_{E2} + \beta_{M2}).
 \tag{34}$$

Here we obtain the following NLO results for the proton and neutron (showing also the separate contributions from πN loops, Δ exchange and $\pi\Delta$ loops), in units of 10^{-4} fm^5 :

$$M_{1p}^{(4)} = 6.00(59) \approx 2.95 + 2.92 + 0.13, \quad (35a)$$

$$M_{1n}^{(4)} = 7.30(72) \approx 4.26 + 2.92 + 0.13. \quad (35b)$$

For the slopes at $Q^2 = 0$, we find, in units of 10^{-4} fm^7 :

$$\left. \frac{dM_{1p}^{(4)}(Q^2)}{dQ^2} \right|_{Q^2=0} = -1.38(14) \approx -1.16 - 0.20 - 0.02, \quad (36a)$$

$$\left. \frac{dM_{1n}^{(4)}(Q^2)}{dQ^2} \right|_{Q^2=0} = -1.96(19) \approx -1.73 - 0.20 - 0.02. \quad (36b)$$

The corresponding individual contributions to the Q^2 dependence of $M_1^{(4)}(Q^2)$ are demonstrated in Fig. 6 {lower panel}.

In Fig. 5 {lower panel}, we show our $B\chi$ PT predictions compared to the MAID model predictions [48–50], the HB limit of the πN -loop contribution [47], and empirical evaluations of the fourth-order Baldin sum rule [37, 66] for proton and neutron, respectively. Our NLO $B\chi$ PT predictions are in good agreement with MAID, while the HB results fail to describe the decrease with growing Q^2 .

E. $\bar{T}_1(0, Q^2)$ — the proton subtraction function

The knowledge of the proton subtraction function $\bar{T}_1(0, Q^2)$ is needed to evaluate the leading contribution of the nucleon structure to the (muonic-)hydrogen Lamb shift, see Refs. [9, 15, 16] for reviews. At very low momenta the non-Born part of the subtraction function is given by the magnetic dipole polarizability, $\bar{T}_1(0, Q^2)/Q^2 = 4\pi\beta_{M1} + \mathcal{O}(Q^2)$. Since the Lamb-shift integrals are weighted towards low Q^2 , the low-momentum features of $\bar{T}_1(0, Q^2)$ have a more pronounced effect. In particular, the uncertainty in the (empirical) extraction of β_{M1} contributes the bulk of the theoretical uncertainty in Ref. [69]. At the same time, the slope of this function at $Q^2 = 0$ could potentially be important, and the different models and mechanisms could lead to rather different values of that slope.

This is illustrated in Fig. 7 {left panel}, which shows the low- Q^2 behavior of $\bar{T}_1(0, Q^2)/4\pi Q^2$. One can see that both β_{M1} and the slope change significantly when one adds the Δ contributions (Δ -exchange and the $\pi\Delta$ loops contribution), cf. Fig. 7 {right panel}. The resulting curve in the left panel is compared with the $HB\chi$ PT evaluation of Ref. [69], showing an appreciable disagreement in the slope, with the Q^2 dependence of the two curves being noticeably different. Our NLO prediction of the slope at $Q^2 = 0$ is given by (in units of 10^{-4} fm^5):

$$\frac{1}{8\pi} \left. \frac{d^2\bar{T}_1(0, Q^2)}{d(Q^2)^2} \right|_{Q^2=0} = -2.33(23) \approx -0.06 - 2.18 - 0.10. \quad (37)$$

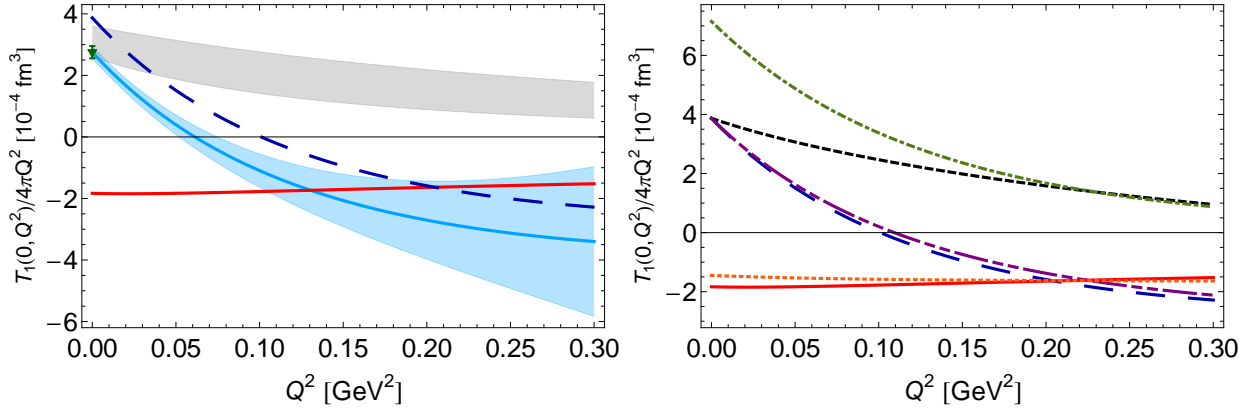


FIG. 7. Left panel: The low- Q^2 behavior of the non-Born piece of subtraction function $\bar{T}_1(0, Q^2)/4\pi Q^2$ for the proton. The result of this work, including the $\delta\beta$ contribution, is shown by the blue solid line, with the blue band representing the uncertainty due to higher-order effects. The blue long-dashed line corresponds to the NLO B χ PT prediction (i.e., without the $\delta\beta$ term). At the real-photon point, we show the value of $\beta_{M1p} = (2.75 \pm 0.2) \times 10^{-4} \text{ fm}^3$ (dark green triangle) resulting from the fit to the Baldin sum rule described in Section III A. The red solid curve corresponds to the B χ PT πN -loop contribution only, the gray band is the HB χ PT evaluation [69]. Right panel: Contributions of the different orders to the chiral prediction of $\bar{T}_1(0, Q^2)/4\pi Q^2$ for the proton. Red solid line: πN -loop contribution, green dot-dashed line: Δ -exchange contribution, orange dotted line: $\pi\Delta$ -loop contribution, blue long-dashed line: total result, purple dot-dot-dashed line: total result without g_C contribution, black short-dashed line: total result without g_M dipole.

Extracting the slope of the subtraction function experimentally should in principle be possible through dilepton electroproduction as proposed in Ref. [20]. It remains to be seen whether such a measurement is feasible in the near future.

V. SUMMARY AND CONCLUSIONS

We have completed the NLO calculation of the unpolarized VVCS amplitudes in SU(2) B χ PT, with explicit $\Delta(1232)$. We have calculated the non-Born amplitudes, which at this order come out as a parameter-free prediction of B χ PT. These amplitudes are used to examine several notable combinations of the (generalized) polarizabilities that are expressed through the moments of the nucleon structure functions, i.e.: $M_1^{(2)}(Q^2)$ — the generalized Baldin sum rule, $M_1^{(4)}(Q^2)$ — the generalized fourth-order Baldin sum rule, $\alpha_L(Q^2)$ — the longitudinal polarizability, and $M_2^{(1)}(Q^2)$ — the first moment of the structure function $F_2(x, Q^2)$. The dispersion relations between the VVCS amplitudes and the tree-level photoabsorption cross sections served as a cross-check of these calculations.

These results can be compared with the dispersive evaluations using the empirical parametrization of the nucleon structure functions. The biggest discrepancy is observed

for the low- Q behavior of the generalized Baldin sum rule, calling for a future revision of the low-momentum behavior of the empirical parametrization of the structure function $F_1(x, Q^2)$.

Concerning the $\Delta(1232)$ contribution, we have seen that it plays an important role in transverse quantities, whereas in the longitudinal quantities, such as the longitudinal polarizability α_L , its role is negligible. The Coulomb $\gamma^*N \rightarrow \Delta$ transition coupling g_C has generally a small effect in the unpolarized moments considered here.

We have also obtained an NLO prediction for the proton subtraction function $\bar{T}_1(0, Q^2)$, which cannot be deduced from dispersion relations. This is an important step towards a systematic improvement of the LO χ PT evaluation [28] of the proton polarizability contribution to the muonic-hydrogen Lamb shift.

ACKNOWLEDGEMENTS

We thank Lothar Tiator and Marc Vanderhaeghen for helpful discussions. This work is supported by the Deutsche Forschungsgemeinschaft (DFG) through the Collaborative Research Center [The Low-Energy Frontier of the Standard Model (SFB 1044)]. JMA acknowledges support from the Community of Madrid through the ‘‘Programa de atracci3n de talento investigador 2017 (Modalidad 1)’’, and the Spanish MECED grants FPA2016-77313-P. FH gratefully acknowledges financial support from the Swiss National Science Foundation.

Appendix A: Photoabsorption cross sections

The forward CS amplitude can, up to the subtraction function, be reconstructed from the total photoabsorption cross sections through the dispersion relations in Eq. (4). Therefore, we use tree-level cross sections to verify our NLO calculation of the non-Born VVCS amplitudes.

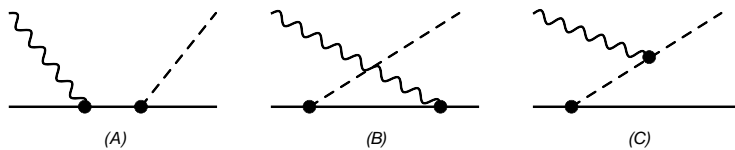


FIG. 8. Contribution of the $\gamma^*N \rightarrow \pi N$ channel to photoabsorption on the nucleon.

At LO, we need to consider the πN -production channel. Following Refs. [32, 70] and performing a chiral rotation to cancel exactly the Kroll-Ruderman term at this order, only the tree-level diagrams shown in Fig. 8 contribute, which are gauge invariant by themselves. Analytical expressions for $\sigma_T(\nu, Q^2)$ and $\sigma_L(\nu, Q^2)$ can be found in Ref. [28]. The cross sections in the real-photon limit can be found in Refs. [32, 70]. We checked that the non-Born VVCS amplitudes at LO, the left-hand side of Eq. (4), are reproduced by the right-hand side of the same equation when the tree-level πN -production photoabsorption cross sections are inserted.

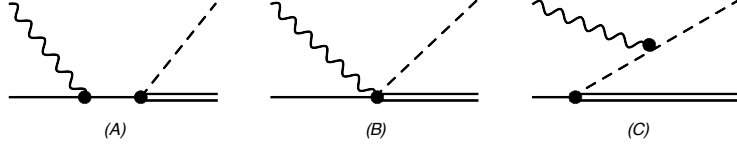


FIG. 9. Contribution of the $\gamma^* N \rightarrow \pi \Delta$ channel to photoabsorption on the nucleon.

Besides the πN production, we calculated the tree-level $\pi \Delta$ -production and Δ -production photoabsorption cross sections, see Figs. 9 and 10. Due to the worse high-energy behavior of the $\pi \Delta$ -production cross sections, cf. Fig. 11, the dispersion relations require further subtractions for a reconstruction of the $\pi \Delta$ -loop contribution to the VVCS amplitudes. However, we could use these cross sections to verify higher-order terms in the expansion of the VVCS amplitudes in powers of small ν .

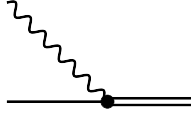


FIG. 10. Contribution of the $\gamma^* N \rightarrow \Delta$ channel to photoabsorption on the nucleon.

The Δ -production cross sections are related to the tree-level Δ -exchange shown in Fig. 2. The threshold for production of the $\Delta(1232)$ -resonance is at lab-frame photon energies of:

$$\nu_{\Delta} = \frac{M_{\Delta}^2 - M_N^2 + Q^2}{2M_N}. \quad (\text{A1})$$

Therefore, the Δ -production cross sections contain to the following Dirac's $\delta(\nu - \nu_{\Delta})$.

The explicit form of these cross sections is given by:

$$\begin{aligned} \sigma_T(\nu, Q^2) = \frac{4\pi^2\alpha}{2M_N M_+^2 |\vec{q}|} & \left\{ g_M^2 |\vec{q}|^2 (\nu + M_+) + \frac{g_E^2 (\nu - \Delta) (M_N \nu - Q^2)^2}{M_N^2} \right. \\ & + \frac{g_C^2 Q^4 s (\nu - \Delta)}{M_N^2 M_{\Delta}^2} - \frac{g_M g_E |\vec{q}|^2 (M_N \nu - Q^2)}{M_N} + \frac{g_M g_C |\vec{q}|^2 Q^2}{M_N} \\ & \left. + \frac{2g_E g_C Q^2 (M_N \nu - Q^2) [-M_{\Delta} (M_N + \nu) + s]}{M_N^2 M_{\Delta}} \right\} \delta(\nu - \nu_{\Delta}), \end{aligned} \quad (\text{A2a})$$

$$\begin{aligned} \sigma_L(\nu, Q^2) = \frac{4\pi^2\alpha}{2M_N^3 M_+^2 |\vec{q}|} & \left\{ g_E^2 (\nu - \Delta) [M_N^2 |\vec{q}|^2 - (Q^2 - M_N \nu)^2] \right. \\ & + \frac{g_C^2 Q^2 (\nu - \Delta) (M_N^2 |\vec{q}|^2 - Q^2 s)}{M_{\Delta}^2} \\ & \left. - \frac{2g_E g_C Q^2 (M_N \nu - Q^2) [s - M_{\Delta} (M_N + \nu)]}{M_{\Delta}} \right\} \delta(\nu - \nu_{\Delta}), \end{aligned} \quad (\text{A2b})$$

with $\Delta = M_{\Delta} - M$, $M_+ = M_{\Delta} + M$ and the Mandelstam variable $s = M_N^2 + 2M_N \nu - Q^2$. Analytical expressions for the unpolarized structure functions can be constructed with the help of Eq. (2), with the flux factor $K(\nu, Q^2) = \sqrt{\nu^2 + Q^2}$.

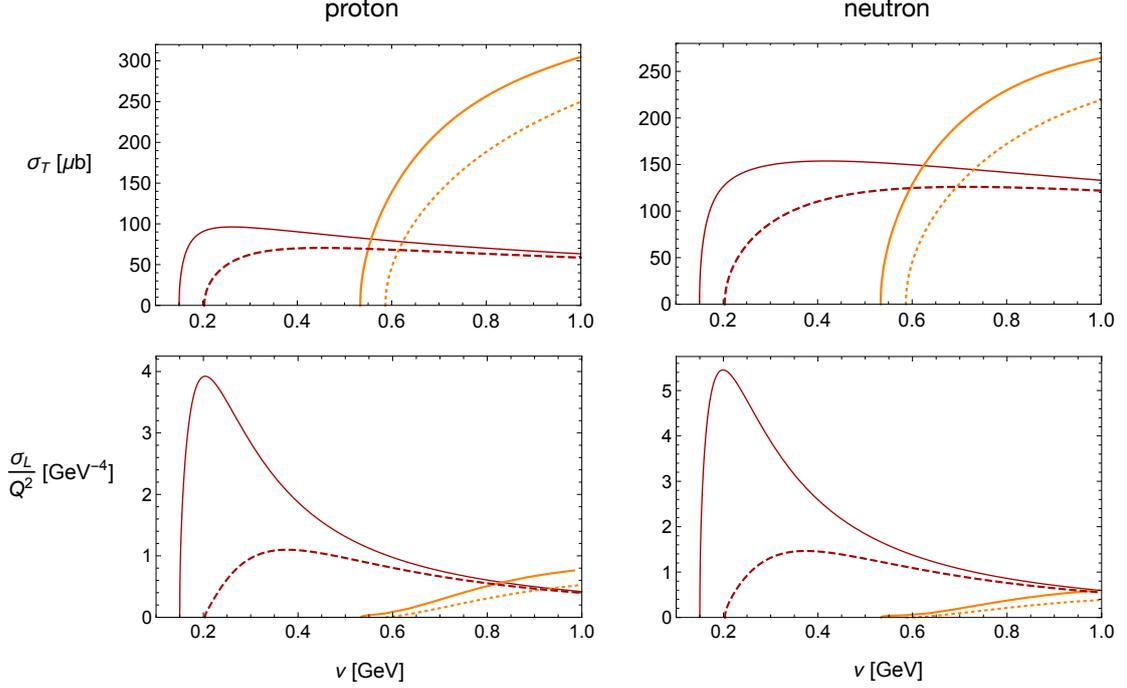


FIG. 11. Photoabsorption cross sections for πN (red) and $\pi\Delta$ production (orange) with $Q^2 = 0$ (solid) and $Q^2 = 0.1 \text{ GeV}^2$ (dashed for πN and dotted for $\pi\Delta$ channel).

It is important to note that the above cross sections only describe the Δ -pole contributions to the tree-level Δ exchange. In general, the VVCS amplitudes described by the Δ -exchange diagram in Fig. 2 can be split as follows [71]:

$$\bar{T}_1^{\Delta\text{-exch.}}(\nu, Q^2) = \bar{T}_1^{\Delta\text{-exch.}}(0, Q^2) + T_1^{\Delta\text{-pole}}(\nu, Q^2) + \tilde{T}_1^{\Delta\text{-exch.}}(\nu, Q^2), \quad (\text{A3a})$$

$$\bar{T}_2^{\Delta\text{-exch.}}(\nu, Q^2) = T_2^{\Delta\text{-pole}}(\nu, Q^2) + \tilde{T}_2^{\Delta\text{-exch.}}(\nu, Q^2). \quad (\text{A3b})$$

$\bar{T}_1^{\Delta\text{-exch.}}(0, Q^2)$ is the usual subtraction function:

$$\begin{aligned} \bar{T}_1^{\Delta\text{-exch.}}(0, Q^2) = \frac{4\pi\alpha Q^4}{M_\Delta M_+ \omega_+} & \left[\frac{g_M^2}{Q^2} - \frac{g_E^2 \Delta}{M_N^2 M_+} - \frac{g_C^2 \Delta (M_N^2 - Q^2)}{M_N^2 M_\Delta^2 M_+} + \frac{g_M g_E}{M_N M_+} + \frac{g_M g_C}{M_N M_+} \right. \\ & \left. + \frac{2g_E g_C (M_N \Delta + Q^2)}{M_N^2 M_\Delta M_+} \right]. \end{aligned} \quad (\text{A4})$$

with $\omega_\pm = (M_\Delta^2 - M^2 \pm Q^2)/2M_\Delta$. $T_i^{\Delta\text{-pole}}$ are the Δ -pole contributions which feature a pole at the $\Delta(1232)$ -production threshold, and thus, are proportional to:

$$\frac{1}{[s - M_\Delta^2][u - M_\Delta^2]} = \frac{1}{4M_N^2} \frac{1}{\nu_\Delta^2 - \nu^2}, \quad (\text{A5})$$

where s and u are the usual Mandelstam variables. $\tilde{T}_i^{\Delta\text{-exch.}}$ are the (Δ -)non-pole terms in which

the pole has cancelled out [71]:

$$\tilde{T}_1^{\Delta\text{-exch.}}(\nu, Q^2) = -\frac{4\pi\alpha\nu^2}{M_N M_+^2} (g_M^2 + g_E^2 - g_M g_E), \quad (\text{A6a})$$

$$\tilde{T}_2^{\Delta\text{-exch.}}(\nu, Q^2) = -\frac{4\pi\alpha Q^2}{M_N M_+^2} \left(g_M^2 + g_E^2 - g_M g_E + \frac{g_C^2 Q^2}{M_\Delta^2} \right). \quad (\text{A6b})$$

To describe the non-pole terms in Eqs. (A6a) and (A6b) within the standard dispersive framework, Eq. (4), we define the auxiliary structure functions:

$$\tilde{F}_1(x, Q^2) = \frac{M_N x}{8\pi\alpha} \tilde{T}_1^{\Delta\text{-exch.}}(x, Q^2) \delta(x), \quad (\text{A7a})$$

$$\tilde{F}_2(x, Q^2) = \frac{Q^2}{16\pi\alpha M_N} \tilde{T}_2^{\Delta\text{-exch.}}(x, Q^2) \delta(x). \quad (\text{A7b})$$

Appendix B: Polarizabilities at $Q^2 = 0$

In this section, we give analytical expressions for the static values and slopes at $Q^2 = 0$ of the polarizabilities and moments of structure functions. In particular, we give the HB expansion of the πN -loop contributions and the Δ -exchange contributions. The complete expressions, also for the $\pi\Delta$ -loop contributions, can be found in the *Supplemented material*.

1. πN -loop contribution

Here, we give analytical expressions for the πN -loop contributions to the proton and neutron polarizabilities, expanded in powers of $\mu = m_\pi/M_N$, viz., the HB expansion. Note that we choose to expand here to a high order in μ , the strict HB expansion would only retain the leading term in an analogous NLO calculation.

- Static polarizabilities ($Q^2 = 0$):

$$\alpha_{E1p} + \beta_{M1p} = \frac{e^2 g_A^2}{96\pi^3 f_\pi^2 m_\pi} \left\{ \frac{11\pi}{8} + 6(3 \log \mu + 4)\mu - \frac{1521\pi\mu^2}{64} - \frac{(210 \log \mu + 29)\mu^3}{3} + \dots \right\}, \quad (\text{B1})$$

$$\alpha_{E1n} + \beta_{M1n} = \frac{e^2 g_A^2}{96\pi^3 f_\pi^2 m_\pi} \left\{ \frac{11\pi}{8} + \frac{(12 \log \mu + 1)\mu}{2} - \frac{117\pi\mu^2}{64} + \frac{7\mu^3}{3} + \dots \right\}, \quad (\text{B2})$$

$$\alpha_{Lp} = \frac{e^2 g_A^2}{1440\pi^3 f_\pi^2 m_\pi^3} \left\{ \frac{93\pi}{32} - \frac{89\mu}{2} + \frac{18231\pi\mu^2}{256} + 10(44 + 51 \log \mu)\mu^3 - \frac{1880805\pi\mu^4}{4096} - 3 \left(356 \log \mu - \frac{129}{10} \right) \mu^5 + \dots \right\}, \quad (\text{B3})$$

$$\alpha_{Ln} = \frac{e^2 g_A^2}{1440\pi^3 f_\pi^2 m_\pi^3} \left\{ \frac{93\pi}{32} - \frac{35}{2}\mu + \frac{4095\pi\mu^2}{256} + \frac{1}{2}(11 + 120 \log \mu)\mu^3 - \frac{80085\pi\mu^4}{4096} + \frac{141\mu^5}{5} + \dots \right\}, \quad (\text{B4})$$

$$M_{1p}^{(4)}(0) = \frac{e^2 g_A^2}{720\pi^3 f_\pi^2 m_\pi^3} \left\{ \frac{81\pi}{32} - 56\mu + \frac{29145\pi\mu^2}{256} + \frac{3}{4} (1501 + 1380 \log \mu) \mu^3 - \frac{4670925\pi\mu^4}{4096} - \frac{96}{5} (13 + 160 \log \mu) \mu^5 + \dots \right\}, \quad (\text{B5})$$

$$M_{1n}^{(4)}(0) = \frac{e^2 g_A^2}{720\pi^3 f_\pi^2 m_\pi^3} \left\{ \frac{81\pi}{32} - 28\mu + \frac{6525\pi\mu^2}{256} + 3(1 + 30 \log \mu) \mu^3 - \frac{113925\pi\mu^4}{4096} + \frac{192\mu^5}{5} + \dots \right\}. \quad (\text{B6})$$

- Slopes of polarizabilities at $Q^2 = 0$:

$$\frac{d(\alpha_{E1p} + \beta_{M1p})(0)}{dQ^2} = \frac{e^2 g_A^2}{480\pi^3 f_\pi^2 m_\pi^3} \left\{ \frac{3\pi}{16} - 18\mu + \frac{6477\pi\mu^2}{128} + \left(\frac{1339}{2} + 550 \log \mu \right) \mu^3 - \frac{1366515\pi\mu^4}{2048} - 7 \left(\frac{313}{10} + 270 \log \mu \right) \mu^5 + \dots \right\}, \quad (\text{B7})$$

$$\frac{d(\alpha_{E1n} + \beta_{M1n})(0)}{dQ^2} = \frac{e^2 g_A^2}{1440\pi^3 f_\pi^2 m_\pi^3} \left\{ \frac{9\pi}{16} - \frac{89\mu}{2} + \frac{5535\pi\mu^2}{128} + (1 + 150 \log \mu) \mu^3 - \frac{92265\pi\mu^4}{2048} + \frac{1209\mu^5}{20} + \dots \right\}, \quad (\text{B8})$$

$$\frac{d\alpha_{Lp}(0)}{dQ^2} = \frac{e^2 g_A^2}{1440\pi^3 f_\pi^2 m_\pi^5} \left\{ -\frac{621\pi}{896} + \frac{13\mu}{14} + \frac{4995\pi\mu^2}{1024} - \frac{669\mu^3}{7} + \frac{2517315\pi\mu^4}{16384} + \left(\frac{34407}{35} + 1116 \log \mu \right) \mu^5 + \dots \right\}, \quad (\text{B9})$$

$$\frac{d\alpha_{Ln}(0)}{dQ^2} = \frac{e^2 g_A^2}{1440\pi^3 f_\pi^2 m_\pi^5} \left\{ -\frac{621\pi}{896} - \frac{55\mu}{14} + \frac{3195\pi\mu^2}{1024} - \frac{207\mu^3}{7} + \frac{456915\pi\mu^4}{16384} + \frac{18}{35} (29 + 210 \log \mu) \mu^5 + \dots \right\}, \quad (\text{B10})$$

$$\frac{dM_{2p}^{(1)}(0)}{dQ^2} = \frac{e^2 g_A^2}{480\pi^3 f_\pi^2 m_\pi^3} \left\{ -\frac{17\pi}{32} + \frac{9\mu}{2} - \frac{399\pi\mu^2}{256} + \frac{1}{3} (197 + 90 \log \mu) \mu^3 - \frac{246015\pi\mu^4}{4096} - \frac{1}{5} (199 + 990 \log \mu) \mu^5 + \dots \right\}, \quad (\text{B11})$$

$$\frac{dM_{2n}^{(1)}(0)}{dQ^2} = \frac{e^2 g_A^2}{480\pi^3 f_\pi^2 m_\pi^3} \left\{ -\frac{17\pi}{32} - 2\mu + \frac{705\pi\mu^2}{256} + \frac{1}{6} (1 + 60 \log \mu) \mu^3 - \frac{12255\pi\mu^4}{4096} + \frac{79\mu^5}{20} + \dots \right\}, \quad (\text{B12})$$

$$\frac{dM_{1p}^{(4)}(0)}{dQ^2} = \frac{e^2 g_A^2}{10080\pi^3 f_\pi^2 m_\pi^5} \left\{ \frac{225\pi}{128} - 229\mu + \frac{495555\pi\mu^2}{1024} - 7542\mu^3 + \frac{217523775\pi\mu^4}{16384} + 3(38771 + 37408 \log \mu) \mu^5 + \dots \right\}, \quad (\text{B13})$$

$$\frac{dM_{1n}^{(4)}(0)}{dQ^2} = \frac{e^2 g_A^2}{2520\pi^3 f_\pi^2 m_\pi^5} \left\{ \frac{225\pi}{512} - \frac{209\mu}{4} + \frac{228795\pi\mu^2}{4096} - \frac{1653\mu^3}{4} + \frac{21341775\pi\mu^4}{65536} + 3(3 + 364 \log \mu) \mu^5 + \dots \right\}. \quad (\text{B14})$$

2. Δ -exchange contribution

Here, we give analytical expressions for the tree-level Δ -exchange contributions, cf. Fig. 2, to the nucleon polarizabilities and their slopes at $Q^2 = 0$. Note that the Δ -exchange contributes equally to proton and neutron polarizabilities. Recall that for the magnetic $\gamma^*N\Delta$ coupling we introduced a dipole form factor to mimic vector-meson dominance: $g_M \rightarrow g_M/(1 + Q^2/\Lambda^2)^2$.

- Static polarizabilities ($Q^2 = 0$):

$$\alpha_{E1} = -\frac{e^2 g_E^2}{2\pi M_+^3}, \quad (\text{B15})$$

$$\beta_{M1} = \frac{e^2 g_M^2}{2\pi M_+^2} \frac{1}{\Delta}, \quad (\text{B16})$$

$$\alpha_L = \frac{e^2 M_\Delta^2}{\pi M_+^3} \left(\frac{g_E^2}{\Delta M_N M_+^2} - \frac{g_C^2}{2M_\Delta^4} + \frac{g_E g_C}{M_N M_\Delta^2 M_+} \right), \quad (\text{B17})$$

$$M_1^{(4)}(0) = \frac{e^2 M_N}{\pi M_+^3 \Delta} \left(\frac{g_M^2}{\Delta^2} + \frac{g_E^2}{M_+^2} - \frac{g_E g_M}{\Delta M_+} \right). \quad (\text{B18})$$

- Slopes of polarizabilities at $Q^2 = 0$:

$$\begin{aligned} \frac{d[\alpha_{E1} + \beta_{M1}](0)}{dQ^2} &= -\frac{e^2}{\pi M_+^2} \left(\frac{g_M^2}{\Delta^2} \left[\frac{1}{M_+} - \frac{1}{2\Delta} \right] + \frac{2}{\Lambda^2} \frac{g_M^2}{\Delta} + \frac{g_M g_E}{M_N} \left[\frac{1}{4\Delta^2} - \frac{1}{\Delta M_+} \right. \right. \\ &\quad \left. \left. + \frac{1}{4M_+^2} \right] - \frac{g_E^2}{4M_N M_+} \left[\frac{1}{\Delta} - \frac{5}{M_+} \right] - \frac{g_M g_C}{2\Delta M_N M_+} + \frac{g_E g_C}{M_N M_+^2} \right), \quad (\text{B19}) \end{aligned}$$

$$\begin{aligned} \frac{d\alpha_L(0)}{dQ^2} &= \frac{e^2 M_\Delta^3}{\pi \Delta M_+^4} \left(\frac{2g_E^2}{\Delta^2 M_+^2} \left[\frac{2}{M_\Delta} - \frac{1}{M_N} \right] - \frac{g_C^2}{M_\Delta^4} \left[\frac{1}{M_N} - \frac{3}{2M_\Delta} \right] \right. \\ &\quad \left. + \frac{g_E g_C}{\Delta M_\Delta^2 M_+} \left[\frac{5}{M_\Delta} - \frac{3}{M_N} \right] \right), \quad (\text{B20}) \end{aligned}$$

$$\begin{aligned} \frac{dM_2^{(1)}(0)}{dQ^2} &= \frac{e^2}{\pi M_+^3} \left(-\frac{g_M^2}{2\Delta^2} - \frac{2g_M^2 M_+}{\Lambda^2 \Delta} + \frac{g_M g_E}{2\Delta M_N} + \frac{g_E^2}{2\Delta M_+} + \frac{g_M g_C}{2\Delta M_N} \right. \\ &\quad \left. - \frac{g_C^2}{2M_\Delta^2} \right), \quad (\text{B21}) \end{aligned}$$

$$\begin{aligned} \frac{dM_1^{(4)}(0)}{dQ^2} &= \frac{e^2 M_N}{\pi \Delta^2 M_+^5} \left(\frac{g_M^2}{\Delta} \left[2 - \frac{5M_+}{\Delta} + \frac{M_+^2}{\Delta^2} \right] - \frac{4M_+^2}{\Delta} \frac{g_M^2}{\Lambda^2} + g_M g_E \left[\frac{6}{\Delta} \right. \right. \\ &\quad \left. \left. - \frac{M_+}{\Delta^2} - \frac{1}{M_+} \right] + \frac{2M_+ g_M g_E}{\Lambda^2} + g_E^2 \left[\frac{1}{\Delta} - \frac{7}{M_+} \right] + \frac{2g_M g_C}{\Delta} \right. \\ &\quad \left. - \frac{4g_E g_C}{M_+} \right). \quad (\text{B22}) \end{aligned}$$

-
- [1] M. Gell-Mann, M. L. Goldberger, and W. E. Thirring, *Phys. Rev.* **95**, 1612 (1954).
- [2] H. Burkhardt and W. N. Cottingham, *Annals Phys.* **56**, 453 (1970).
- [3] J. Schwinger, *Proc. Natl. Acad. Sci. USA* **72**, 1559 (1975).
- [4] J. Bernabeu and R. Tarrach, *Phys. Lett.* **B 55**, 183 (1975).
- [5] A. I. L’vov, *Nucl. Phys.* **A 638**, 756 (1998).
- [6] D. Drechsel, B. Pasquini, and M. Vanderhaeghen, *Phys. Rept.* **378**, 99 (2003), [hep-ph/0212124](#).
- [7] S. E. Kuhn, J.-P. Chen, and E. Leader, *Prog. Part. Nucl. Phys.* **63**, 1 (2009), [arXiv:0812.3535 \[hep-ph\]](#).
- [8] B. R. Holstein and S. Scherer, *Ann. Rev. Nucl. Part. Sci.* **64**, 51 (2014), [arXiv:1401.0140 \[hep-ph\]](#).
- [9] F. Hagelstein, R. Miskimen, and V. Pascalutsa, *Prog. Part. Nucl. Phys.* **88**, 29 (2016), [arXiv:1512.03765 \[nucl-th\]](#).
- [10] V. Pascalutsa, *Causality Rules*, IOP Concise Physics (Morgan & Claypool Publishers, 2018).
- [11] B. Pasquini and M. Vanderhaeghen, *Ann. Rev. Nucl. Part. Sci.* **68**, 75 (2018), [arXiv:1805.10482 \[hep-ph\]](#).
- [12] R. Pohl *et al.*, *Nature* **466**, 213 (2010).
- [13] A. Antognini, F. Nez, K. Schuhmann, F. D. Amaro, *et al.*, *Science* **339**, 417 (2013).
- [14] R. Pohl *et al.* (CREMA), *Science* **353**, 669 (2016).
- [15] R. Pohl, R. Gilman, G. A. Miller, and K. Pachucki, *Ann. Rev. Nucl. Part. Sci.* **63**, 175 (2013), [arXiv:1301.0905 \[physics.atom-ph\]](#).
- [16] C. E. Carlson, *Prog. Part. Nucl. Phys.* **82**, 59 (2015), [arXiv:1502.05314 \[hep-ph\]](#).
- [17] R. Pohl *et al.*, *Proceedings, 12th International Conference on Low Energy Antiproton Physics (LEAP2016), Kanazawa, Japan, March 6-11, 2016*, *JPS Conf. Proc.* **18**, 011021 (2017), [arXiv:1609.03440 \[physics.atom-ph\]](#).
- [18] D. Bakalov, A. Adamczak, M. Stoilov, and A. Vacchi, *Proceedings, 5th International Conference on Exotic Atoms and Related Topics (EXA2014): Vienna, Austria, September 15-19, 2014*, *Hyperfine Interact.* **233**, 97 (2015).
- [19] S. Kanda *et al.*, *J. Phys. Conf. Ser.* **1138**, 012009 (2018).
- [20] V. Pauk, C. E. Carlson, and M. Vanderhaeghen, (2020), [arXiv:2001.10626 \[hep-ph\]](#).
- [21] S. Weinberg, *Physica* **A 96**, 327 (1979).
- [22] J. Gasser and H. Leutwyler, *Ann. Phys.* **158**, 142 (1984).
- [23] J. Gasser, M. E. Sainio, and A. Švarc, *Nucl. Phys.* **B 307**, 779 (1988).
- [24] J. Gegelia and G. Japaridze, *Phys. Rev.* **D 60**, 114038 (1999), [arXiv:hep-ph/9908377](#).
- [25] T. Fuchs, J. Gegelia, G. Japaridze, and S. Scherer, *Phys. Rev.* **D 68**, 056005 (2003), [arXiv:hep-ph/0302117](#).
- [26] V. Pascalutsa and D. R. Phillips, *Phys. Rev.* **C 67**, 055202 (2003), [arXiv:nucl-th/0212024](#).
- [27] V. Lensky, J. M. Alarcón, and V. Pascalutsa, *Phys. Rev.* **C 90**, 055202 (2014), [arXiv:1407.2574](#)

- [hep-ph].
- [28] J. M. Alarcón, V. Lensky, and V. Pascalutsa, *Eur. Phys. J. C* **74**, 2852 (2014), arXiv:1312.1219 [hep-ph].
- [29] J. Gasser, H. Leutwyler, and A. Rusetsky, (2020), arXiv:2003.13612 [hep-ph].
- [30] A. M. Baldin, *Nucl. Phys.* **18**, 310 (1960).
- [31] V. Lensky, F. Hagelstein, V. Pascalutsa, and M. Vanderhaeghen, *Phys. Rev. D* **97**, 074012 (2018), arXiv:1712.03886 [hep-ph].
- [32] V. Lensky and V. Pascalutsa, *Eur. Phys. J. C* **65**, 195 (2010).
- [33] V. Lensky, J. McGovern, and V. Pascalutsa, *Eur. Phys. J. C* **75**, 604 (2015), arXiv:1510.02794 [hep-ph].
- [34] V. Lensky, V. Pascalutsa, and M. Vanderhaeghen, *Eur. Phys. J. C* **77**, 119 (2017), arXiv:1612.08626 [hep-ph].
- [35] V. Pascalutsa, M. Vanderhaeghen, and S. N. Yang, *Phys. Rept.* **437**, 125 (2007), arXiv:hep-ph/0609004.
- [36] L. Geng, *Front. Phys. China* **8**, 328 (2013), arXiv:1301.6815 [nucl-th].
- [37] O. Gryniuk, F. Hagelstein, and V. Pascalutsa, *Phys. Rev. D* **92**, 074031 (2015), arXiv:1508.07952 [nucl-th].
- [38] M. I. Levchuk and A. I. L'vov, *Nucl. Phys. A* **674**, 449 (2000), nucl-th/9909066.
- [39] V. Lensky and J. A. McGovern, *Phys. Rev. C* **89**, 032202 (2014), arXiv:1401.3320 [nucl-th].
- [40] H. Griebhammer, J. McGovern, D. Phillips, *et al.*, *Prog. Part. Nucl. Phys.* **67**, 841 (2012), arXiv:1203.6834 [nucl-th].
- [41] L. S. Myers *et al.*, *Phys. Rev. Lett.* **113**, 262506 (2014), arXiv:1409.3705 [nucl-ex].
- [42] V. Pascalutsa and M. Vanderhaeghen, *Phys. Rev. D* **73**, 034003 (2006), arXiv:hep-ph/0512244.
- [43] V. Pascalutsa and M. Vanderhaeghen, *Phys. Rev. Lett.* **95**, 232001 (2005), arXiv:hep-ph/0508060.
- [44] K. A. Olive *et al.* (Particle Data Group), *Chin. Phys. C* **38**, 090001 (2014).
- [45] F. E. Low, *Phys. Rev.* **96**, 1428 (1954).
- [46] M. Gell-Mann and M. L. Goldberger, *Phys. Rev.* **96**, 1433 (1954).
- [47] D. Nevado and A. Pineda, *Phys. Rev. C* **77**, 035202 (2008), arXiv:0712.1294 [hep-ph].
- [48] D. Drechsel, S. S. Kamalov, and L. Tiator, *Phys. Rev. D* **63**, 114010 (2001), arXiv:hep-ph/0008306.
- [49] D. Drechsel, O. Hanstein, S. S. Kamalov, and L. Tiator, *Nucl. Phys. A* **645**, 145 (1999), arXiv:nucl-th/9807001.
- [50] L. Tiator, “private communication,” (2020).
- [51] Y. Liang, M. Christy, R. Ent, and C. Keppel, *Phys. Rev. C* **73**, 065201 (2006), arXiv:nucl-ex/0410028.
- [52] J. Bernabeu and T. E. O. Ericson, *Z. Phys. A* **309**, 213 (1983).
- [53] K. Pachucki, *Phys. Rev. A* **53**, 2092 (1996).
- [54] C. E. Carlson and M. Vanderhaeghen, *Phys. Rev. A* **84**, 020102 (2011), arXiv:1101.5965 [hep-ph].

- [55] D. Babusci, G. Giordano, and G. Matone, *Phys. Rev. C* **57**, 291 (1998), [arXiv:nucl-th/9710017](#).
- [56] C. Peset and A. Pineda, *Eur. Phys. J. A* **51**, 32 (2015), [arXiv:1403.3408 \[hep-ph\]](#).
- [57] C. Peset and A. Pineda, *Nucl. Phys. B* **887**, 69 (2014), [arXiv:1406.4524 \[hep-ph\]](#).
- [58] V. Bernard, N. Kaiser, and U.-G. Meißner, *Int. J. Mod. Phys. E* **4**, 193 (1995), [arXiv:hep-ph/9501384](#).
- [59] T. R. Hemmert, B. R. Holstein, and J. Kambor, *Phys. Rev. D* **55**, 5598 (1997), [arXiv:hep-ph/9612374](#).
- [60] V. Bernard, N. Kaiser, and U.-G. Meißner, *Phys. Rev. Lett.* **67**, 1515 (1991).
- [61] V. Bernard, N. Kaiser, and U.-G. Meißner, *Nucl. Phys. B* **373**, 346 (1992).
- [62] V. Olmos de León *et al.*, *Eur. Phys. J. A* **10**, 207 (2001).
- [63] J. A. McGovern, D. R. Phillips, and H. W. Griedhammer, *Eur. Phys. J. A* **49**, 12 (2013), [arXiv:1210.4104 \[nucl-th\]](#).
- [64] N. L. Hall, A. W. Thomas, and R. D. Young, *Phys. Rev. D* **89**, 117502 (2014), [arXiv:1401.8062 \[nucl-th\]](#).
- [65] A. Sibirtsev and P. G. Blunden, *Phys. Rev. C* **88**, 065202 (2013), [arXiv:1311.6482 \[nucl-th\]](#).
- [66] U. Schröder, *Nucl. Phys. B* **166**, 103 (1980).
- [67] I. Guiasu and E. Radescu, *Annals Phys.* **120**, 145 (1979).
- [68] B. R. Holstein, D. Drechsel, B. Pasquini, and M. Vanderhaeghen, *Phys. Rev. C* **61**, 034316 (2000), [arXiv:hep-ph/9910427](#).
- [69] M. C. Birse and J. A. McGovern, *Eur. Phys. J. A* **48**, 120 (2012), [arXiv:1206.3030 \[hep-ph\]](#).
- [70] B. R. Holstein, V. Pascalutsa, and M. Vanderhaeghen, *Phys. Rev. D* **72**, 094014 (2005), [arXiv:hep-ph/0507016](#).
- [71] F. Hagelstein, *Proceedings, 11th International Workshop on the Physics of Excited Nucleons (NSTAR 2017): Columbia, SC, USA, August 20-23, 2017*, *Few Body Syst.* **59**, 93 (2018), [arXiv:1801.09790 \[nucl-th\]](#).